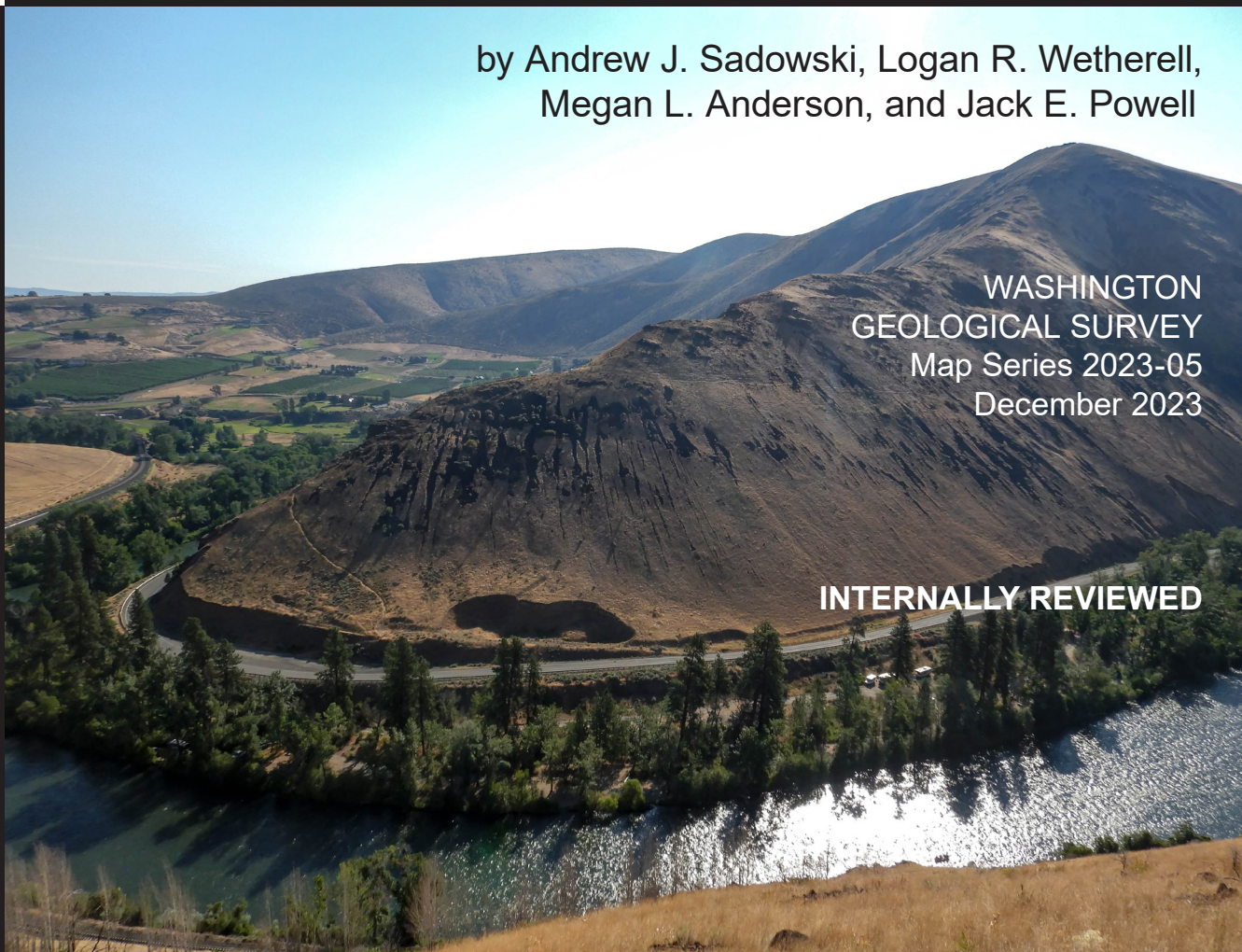


GEOLOGIC MAP OF THE KITTITAS AND EAST KITTITAS 7.5-MINUTE QUADRANGLES, KITTITAS COUNTY, WASHINGTON

by Andrew J. Sadowski, Logan R. Wetherell,
Megan L. Anderson, and Jack E. Powell

WASHINGTON
GEOLOGICAL SURVEY
Map Series 2023-05
December 2023

INTERNALLY REVIEWED



WASHINGTON STATE DEPARTMENT OF
NATURAL RESOURCES
WASHINGTON GEOLOGICAL SURVEY

GEOLOGIC MAP OF THE KITTITAS AND EAST KITTITAS 7.5-MINUTE QUADRANGLES, KITTITAS COUNTY, WASHINGTON

by Andrew J. Sadowski, Logan R. Wetherell,
Megan L. Anderson, and Jack E. Powell

WASHINGTON
GEOLOGICAL SURVEY
Map Series 2023-05
December 2023

*This geologic map was funded in part by
the USGS National Cooperative Geologic
Mapping Program, award no. G22AC00364*

*This publication has been subject to an iterative technical review
process by at least one Survey geologist who is not an author.
This publication has also been subject to an iterative
review process with Survey editors and cartographers.*



WASHINGTON STATE DEPARTMENT OF
NATURAL RESOURCES
WASHINGTON GEOLOGICAL SURVEY

DISCLAIMER

Neither the State of Washington, nor any agency thereof, nor any of their employees, makes any warranty, express or implied, or assumes any legal liability or responsibility for the accuracy, completeness, or usefulness of any information, apparatus, product, or process disclosed, or represents that its use would not infringe privately owned rights. Reference herein to any specific commercial product, process, or service by trade name, trademark, manufacturer, or otherwise, does not necessarily constitute or imply its endorsement, recommendation, or favoring by the State of Washington or any agency thereof. The views and opinions of authors expressed herein do not necessarily state or reflect those of the State of Washington or any agency thereof.

INDEMNIFICATION

Research supported by the U.S. Geological Survey, National Cooperative Geologic Mapping Program, under USGS award number G22AC00364. The views and conclusions contained in this document are those of the authors and should not be interpreted as necessarily representing the official policies, either expressed or implied, of the U.S. Government.

WASHINGTON STATE DEPARTMENT OF NATURAL RESOURCES

Hilary S. Franz—*Commissioner of Public Lands*

WASHINGTON GEOLOGICAL SURVEY

Casey R. Hanell—*State Geologist*

Jessica L. Czajkowski—*Assistant State Geologist*

Ana Shafer—*Assistant State Geologist*

Washington State Department of Natural Resources Washington Geological Survey

Mailing Address:

1111 Washington St SE

MS 47007

Olympia, WA 98504-7007

Street Address:

Natural Resources Bldg, Rm 148

1111 Washington St SE

Olympia, WA 98501

Phone: 360-902-1450

Fax: 360-902-1785

Email: geology@dnr.wa.gov

Website: www.dnr.wa.gov/geology

Publications and Maps:

[www.dnr.wa.gov/programs-and-services/geology/
publications-and-data/publications-and-maps](http://www.dnr.wa.gov/programs-and-services/geology/publications-and-data/publications-and-maps)

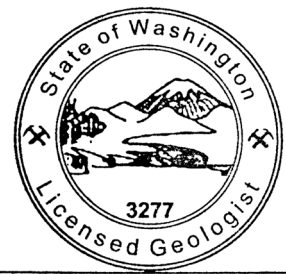
Washington Geology Library Searchable Catalog:

[www.dnr.wa.gov/programs-and-services/geology/
washington-geology-library](http://www.dnr.wa.gov/programs-and-services/geology/washington-geology-library)



Suggested Citation: Sadowski, A. J.; Wetherell, L. R.; Anderson, M. L.; Powell, J. E., 2023, Geologic map of the Kittitas and East Kittitas 7.5-minute quadrangles, Kittitas County, Washington: Washington Geological Survey Map Series 2023-05, 1 sheet, scale 1:24,000, with 32 p. text. [https://www.dnr.wa.gov/publications/ger_ms2023-05_geol_map_kittitas_e_kittitas_24k.zip]

Cover photo: View of Yakima Canyon, looking east toward the Rattlesnake Dance Trail across the Yakima River. Photo by A. Sadowski.



ANDREW JOHN SADOWSKI

Andrew Sadowski

December 2023

Contents

Introduction	1
Geologic Overview	2
Bedrock	2
Surficial Deposits	2
Tectonic Framework	3
Methods	3
Geologic Mapping	3
Data Collection and Analysis	3
Description of Map Units	4
Holocene to Pleistocene Nonglacial Deposits	4
Holocene to Pliocene Nonglacial Alluvial and Colluvial Deposits	5
Tertiary Sedimentary and Volcanic Bedrock	8
Lithologies Depicted as Overlays	16
Mass Wasting (overlay mw)	16
Quaternary Loess (overlay Ql)	16
Miocene Hyaloclastite (overlay hy)	16
Discussion	18
Paleoenvironments of the Upper Ellensburg Formation	18
Description of Geologic Structures	18
Discussion of Geophysical Anomalies	19
Recommendations for Future Research	20
Acknowledgments	20
Author Contributions	21
References	21
Appendix A. Gravity	25
Appendix B. Rock Physical Properties	26
Appendix C. Quantitative Geophysical Modeling of Geologic Cross Sections	27
Appendix D. Geochemistry	28
Appendix E. Geochronology	29

FIGURES

Figure 1. Map of physiographic features, placenames, and roads	2
Figure 2. Composite stratigraphic section of the late Miocene upper Ellensburg Formation ...	7
Figure 3. Annotated panoramic photo of Vanderbilt Gap	17

TABLES

Table 1. Summary of ages	6
Table E1. U-Pb ages	29

MAP SHEET

Geologic Map of the Kittitas and East Kittitas 7.5-minute
Quadrangles, Kittitas County, Washington

Figure M1. Geophysical interpretation for the map area

Geologic Map of the Kittitas and East Kittitas 7.5-minute Quadrangles, Kittitas County, Washington

by Andrew J. Sadowski¹, Logan R. Wetherell¹, Megan L. Anderson¹, and Jack E. Powell¹

¹ Washington Geological Survey
1111 Washington St SE
MS 47007
Olympia, WA 98504-7007

ABSTRACT

New geological and geophysical investigations of the Kittitas and East Kittitas quadrangles refine Neogene stratigraphy and characterize geologic structures in southern Kittitas Valley. New whole rock geochemistry ($n=329$) locally refines the middle Miocene chemostratigraphic framework of the Columbia River Basalt Group (CRBG). These strata are tilted toward Kittitas Valley by faulting and folding at the mountain front. Abundant suprabasalt late Miocene to Pliocene volcanoclastic strata are less steeply tilted.

From twelve U-Pb analyses, we interpret eruptive ages of ~ 15.95 Ma for a tuff at the top of the Vantage Member and ~ 8.72 Ma for a pumice within the upper Ellensburg Formation. Younger sedimentary interbeds of the Ellensburg Formation are more common and thicker compared to older interbeds, suggesting a migrating and (or) deepening depositional center. Between ~ 5.4 and ~ 3.3 Ma, deposition transitioned from largely Cascade-sourced sediments of the Ellensburg Formation to basalt-derived sediments of overlying Pliocene(?)–Quaternary deposits.

We identify reverse and thrust faults with oblique-slip on the flanks of bedrock highs. We interpret these range front faults as young, in-sequence thrust-type structures in a compressional or transpressional regime. Fault-related folds are associated with these structures, including several plunging, northwest- through west-trending anticlines and synclines. We map numerous northerly striking oblique-slip faults with varying offsets, especially where the folds of the Boylston Mountains bend northward.

Geophysical modeling of gravity and aeromagnetic data suggests laterally abrupt thickness changes in basaltic units. These thickness changes may be related to (1) ramp-flat geometries under uplifts; and (or) (2) periods of syn-eruptive development of local accommodation space, where CRBG rocks experienced concurrent footwall thickening (growth strata) and hanging-wall thinning (uplift-related erosion).

INTRODUCTION

The Kittitas and East Kittitas 7.5-minute quadrangles are located in eastern Kittitas County in central Washington State (Fig. 1). This map area covers southern and southeastern Kittitas Valley, which is located east of the Cascade Range on the western edge of the Columbia Basin.

Kittitas Valley is a northwest–southeast trending structural basin bound by fault-related folds and faults (Smith, 1903a, 1903b; Schuster, 1994; Sadowski and others, 2020, 2021, 2022). The map area includes (Fig. 1): (1) the gently southwest-sloping Kittitas Valley bottom in the northwest, (2) the northwest-trending Boylston Mountains with west-draining Wippel Creek in the east, (3) northwest-draining Badger Pocket in the southeast, and (4) west–northwest-trending Manastash Ridge with the south-draining Yakima River in the south–southwest. Mountains obliquely face each other across Badger Pocket and meet southeast of the map area (Fig. 1). I-82/US 97 and SR-821 cross Manastash Ridge at Vanderbilt Gap and the Yakima River, respectively, and

I-90 crosses the northern portion of the Boylston Mountains (Fig. 1).

Our 1:24,000-scale geologic mapping aims to improve understanding of the geologic history of Washington, characterize geologic hazards, and locate natural resources. It builds upon prior geologic mapping at 1:100,000 scale (Waite, 1979; Tabor and others, 1982; Schuster, 1994), nearby 1:24,000-scale mapping (Sadowski and others, 2020, 2021, 2022), detailed surficial mapping by Kelsey and others (2017), and six partially overlapping, unpublished 1:12,000-scale geologic maps by Bentley and Powell from the early 1980s compiled by Schuster (1994). We partially adopted linework from those unpublished maps, with some modification, on our map.

Our work is part of a multi-year geologic mapping project to characterize active faults in the region and better understand how the Yakima fold and thrust belt (YFTB) may transfer strain across the Cascade Range. The new mapping we present will assist in geologic hazard assessment, geotechnical engineering,

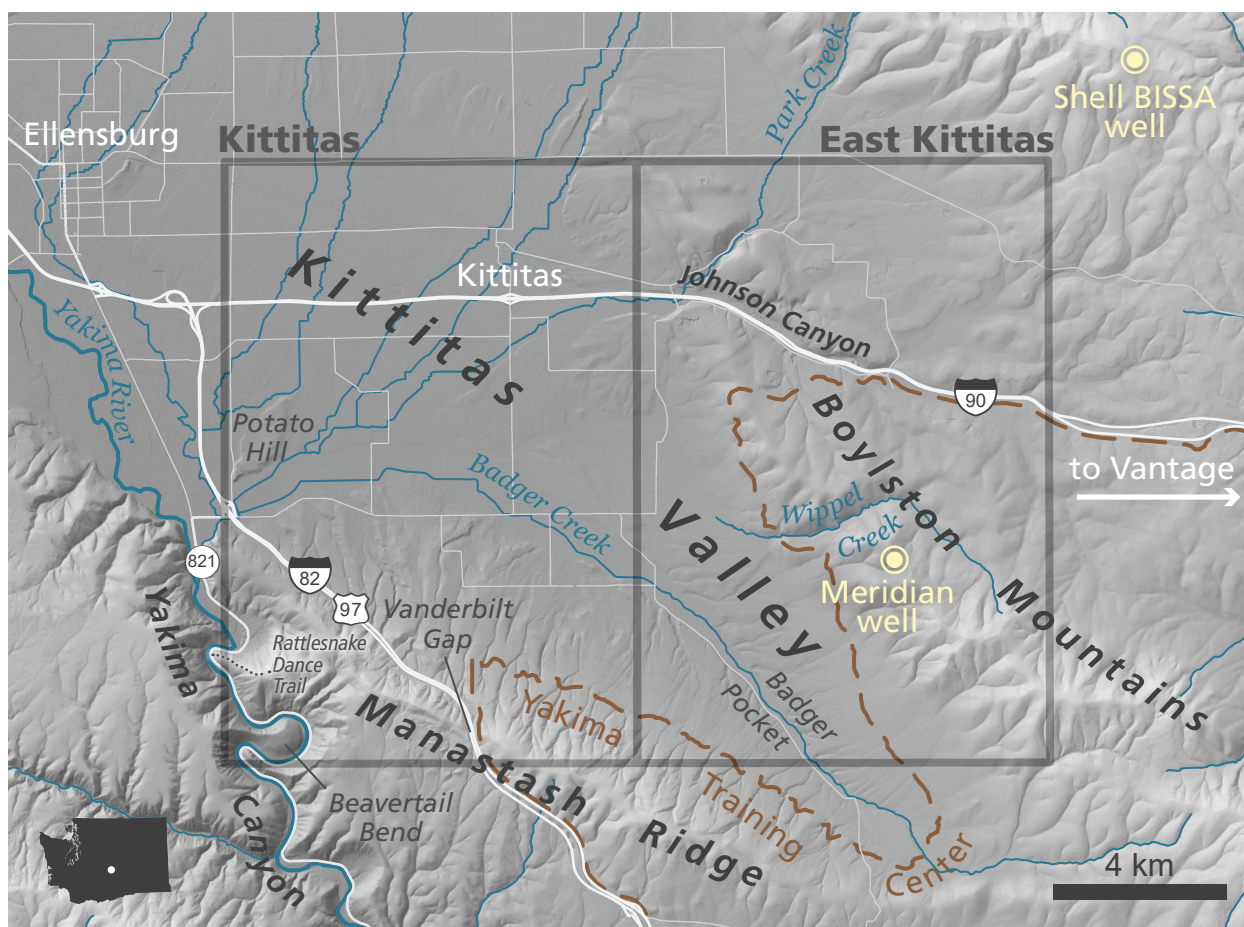


Figure 1. Map of physiographic features, placenames, and roads mentioned in this report, along with the locations of the Shell BISSA and Meridian hydrocarbon exploration wells. Highway 821 is also called Canyon Road.

groundwater hydrology, earth resource management, academic research, and investigations for growth management planning.

GEOLOGIC OVERVIEW

The following *Geologic Overview* and *Methods* sections are largely similar to and summarized from Sadowski and others (2020, 2021, 2022).

Bedrock

Volcanic bedrock is Miocene Grande Ronde Basalt (GRB) and Wanapum Basalt of the Columbia River Basalt Group (CRBG), a continental flood basalt province (Reidel and Tolan, 2013). CRBG lavas were erupted from terrestrial dike swarms in southeast Washington, northeast Oregon, and western Idaho. They flowed great distances until they either cooled on land, or quenched in local water bodies (rivers or lakes) producing pillow breccia, palagonite, and hyaloclastite (Tolan and others, 1989; Reidel and others, 2013a). Roughly 95 percent of the CRBG erupted rapidly between 16.7 and 15.9 Ma (Kasbohm and Schoene, 2018; Kasbohm and others, 2023). The GRB constitutes about 72 percent of the CRBG by volume (Reidel and others, 2013a). Compared to GRB units, Wanapum Basalt units are generally thinner, commonly pinch out laterally, and more commonly contain hyaloclastite.

Volcaniclastic and feldspathic sedimentary rocks of the Ellensburg Formation unconformably overlie and interfinger the CRBG (Schmincke, 1964, 1967a,b; Smith, 1988a,b). The two general sources for these sedimentary rock types are recognized as (1) the ancestral Cascade Range, which provided volcaniclastic detritus to the ancestral Columbia Basin; and (2) ancient rivers of the inland Pacific Northwest (such as the ancestral Columbia River), which provided feldspathic and micaceous material to the ancestral basin from distal sources (Schmincke, 1964, 1967a,b; Smith 1988a,b). The lower Ellensburg Formation includes named, mappable CRBG interbeds—the Coleman (Bentley, 1977), Vantage, and Lmuma Creek members—whereas Miocene to Pliocene(?) sedimentary rocks above CRBG rocks are locally upper Ellensburg Formation.

Surficial Deposits

Within the map area, Pliocene through Holocene nonglacial deposits unconformably rest on Miocene bedrock (Porter, 1976; Waitt, 1979; Sadowski and others 2020, 2021, 2022). Alluvium and colluvial fan deposits with various relative elevations, surface morphologies, and ages are present in the map area; these fans and terraces are composed of either monomictic locally sourced basalt cobbles or polymictic Cascade Range-sourced rocks.

Pleistocene eolian loess of the Palouse Formation is thicker in southern Kittitas Valley compared to northern Kittitas Valley. Deposition of the Palouse Formation involved wind-blown

redistribution of fine-grained sand and silt sourced from ablation till, sandy to silty outwash, and (or) silt of slackwater deposits from cataclysmic floods related to continental glaciations (McDonald and Busacca, 1992).

Landslide deposits and mass-wasting landforms are common along Manastash Ridge and the Boylston Mountains and tend to mantle older units. We map these landforms by their variable, hummocky surface morphologies. The youngest surficial units in the valley are extensively modified by agriculture, irrigation, and aggregate mining.

Tectonic Framework

The map area lies within the modern backarc of the Cascadia subduction zone. During the Eocene, non-marine sediments and volcanic rocks filled backarc structural basins (Tabor and others, 1982; Johnson, 1985; Eddy and others, 2016, 2017; Donaghy and others, 2021). These continental basins were later filled and capped by voluminous Neogene lavas related to hot spot volcanism that was concomitant with the onset of Miocene compression and transpression, a stress regime that resulted from oblique subduction with steady, regional, clockwise rotation of the crust (Reidel and others, 1984; Wells and McCaffrey, 2013; Brocher and others, 2017). Global Positioning System (GPS) velocities reveal that ongoing north–northeast-directed shortening (McCaffrey and others, 2013; Wells and others, 1998) is accommodated by extensive, kilometer-scale, west- and northwest-striking, reverse-to-thrust faults and associated folds of the YFTB (Reidel and others, 2013b; Kelsey and others, 2017; Staisch and others, 2018a,b). Our work encompasses part of the YFTB near Kittitas Valley and builds on prior studies of local active faults by Blakely and others (2011, 2014), Ladinsky and Kelsey (2012), Barnett and others (2013), Bender and others (2016), Kelsey and others (2017), and Staisch and others (2018a,b).

METHODS

Geologic Mapping

We identified lithologic units from field observations in the summer and fall of 2022. We collected over ~3,000 field data points using traditional geological field methods and digitally recorded them with Esri's ArcGIS Field Maps application. We reviewed existing 1:100,000-scale geologic mapping (Waite, 1979; Tabor and others, 1982), six unpublished 1:12,000-scale field map sheets (R. Bentley and J. Powell, Central Washington University, unpub. mapping, 1980–1989), and elevation data from lidar (USACE, 2008). We refer to many geologic structures originally named by Bentley (1977). Near the Yakima River, we adopted the alluvial fan mapping of Kelsey and others (2017) with some modification, and extrapolate their surficial mapping farther southeast along the Manastash range front. We used lidar data to derive slope maps, hillshade images, Red Relief Image Maps (RRIM), and contours. We also used lidar data, recent orthophotos, and historical Google Earth imagery (especially imagery collected in May 2017) to identify probable and certain fault-related lineaments.

We publish 454 bedding attitudes, sedimentary structures, igneous foliations, joints, and faults. We compiled 120 of these

454 measurements with little to no modification from unpublished mapping (R. Bentley and J. Powell, Central Washington University, unpub. mapping, 1980–1989) in the map area, but did not adopt their unit classifications. These compiled measurements are a different color on the map sheet and attributed in the GIS metadata. Due to scale, some measurements have been omitted from the map sheet, but all are available in the GIS data. From structural and map data, we constructed two unbalanced southwest–northeast cross sections. We did not produce a balanced cross section due to limited project time, scope, and geographic extent, and due to the possibility of tectonic movement in and out of the plane of section (see *Discussion*). We encourage future workers to refine fault geometries with our new mapping, geologic attitudes, geophysical data, and rock properties.

We describe flood basalt intraflow textures (physical volcanology), generally found in the following order (from bottom to top): hyaloclastites of pillow-palagonite breccias, basal colonnades, entablatures, internal vesicular zones, vesicular tops, and autobreccias (Reidel, 2015). Intraflow textures help us assess flow-by-flow stratigraphy and choose geochemistry samples that can be compared to previous results (Reidel, 2005; Reidel and Tolan, 2013; Hammond, 2013; Sadowski and others, 2020, 2021, 2022) to elucidate chemostratigraphy. In CRBG rocks, we measure planar orientations of flow foliation surfaces on vesicular and colonnade tops. Similarly, the orientations of upright column sides in colonnade sections are measured and analyzed stereographically using Stereonet 10.1.0 software (Allmendinger and others, 2012; Cardozo and Allmendinger, 2013) to determine cooling surfaces inferred to represent paleo-horizontal. Volcanic flow foliation orientations are generally reliable, but less accurate compared to sedimentary bedding orientations.

Data Collection and Analysis

We reviewed multiple datasets to inform our mapping and subsurface understanding: 46 water well logs, 3 hydrocarbon exploration records—Meridian Oil, Inc. #23-35 BN (API# 046037-00009), Shell BISSA #1-29 (API# 046037-00006), and Yakima Minerals #1-33 (API# 046037-00004)—geophysical data (gravity and aeromagnetic), geochemical analyses (major and trace elements using X-ray fluorescence only), and petrographic analyses of thin sections.

POTENTIAL-FIELDS GEOPHYSICAL METHODS

We combined 352 new gravity observations with 848 observations from previous studies (Sadowski and others, 2020, 2021, 2022) to create a refined isostatic anomaly map of the Kittitas Valley region (Fig. M1A) with approximately 1 km grid spacing. Detailed methods for collecting gravity data, reducing said data, and generating “max-spots” of high-amplitude linear gradients are in Appendix A (Fig. M1A). We also used aeromagnetic data from two surveys (Blakely and others, 2020a,b) to interpret magnetic anomalies related to volcanic bedrock. Aeromagnetic measurements are interpolated to a projected, rectilinear grid using a bi-directional gridding algorithm within the GIS software package Geosoft Oasis Montaj (Seequent, Inc.). We apply a filter that reduces anomalies to the magnetic pole to more closely center them over their sources for map-view interpretation. We interpret

linear anomalies within gravity and aeromagnetic datasets to be related to regionally significant structures.

Gravity measurements spaced 250 m apart along profiles support forward modeling of the gravity and aeromagnetic anomalies along Cross Section A–A' and B–B' using GM-SYS (Geosoft, Inc.; Figs. M1B,C). These models quantitatively test subsurface interpretations developed from map-view data (Appendix C). We calibrate our modeling parameters with published rock properties (Staish and others, 2018a,b), and with our own density and magnetic susceptibility measurements (elsewhere herein, rock properties), including 179 measurements from previous studies (Sadowski and others, 2020, 2021, 2022) and 68 new measurements from this study (Appendix B). Local oil well logs for the Meridian BN #23-35, BISSA #1-29, and Yakima #1-33 (S. Reidel, WSU Tri-Cities, written commun., 2020) and prior modeling in the region (Staish and others, 2018a,b; Blakely and others, 2011) give us estimates of CRBG thickness changes across the region. The Data Supplement contains the tabular gravity and rock property data.

GEOCHEMISTRY

A total of 329 geochemistry samples of basaltic andesite and basalt from the map area were submitted for whole-rock geochemistry (X-ray fluorescence only) to the Peter Hooper GeoAnalytical Lab at Washington State University (WSU) (see Appendix D and Data Supplement). Geochemistry sites G1–G312 are in the map area, whereas sites G313–G330 are outside of the quadrangle to the east or south. These 329 samples include 76 samples collected in 2021 from the East Kittitas quadrangle, which we publish here (see Data Supplement).

Stratigraphic relationships and geochemical variation diagrams (especially TiO_2 vs. MgO , TiO_2 vs. P_2O_5 , and amounts of Zr and Cr) from Hammond (2013) and Sadowski and others (2020, 2021, 2022) aid unit classification. On the map we distinguish individual lava flows of a single geochemically distinct unit where vesicular tops and (or) topographic slope breaks indicate flow boundaries. These boundaries are symbolized as dark gray lines (see 'Geologic Boundary' in the map legend).

We performed an initial classification of our geochemical data using a machine learning (ML) model developed by Dr. Ashley Steiner at the WSU Peter Hooper GeoAnalytical Lab. The ML model does not consider stratigraphic context when making its classifications. As such, we relied less on the ML model classifications and more on elemental variation diagrams and stratigraphic relationships to determine the most reasonable unit classifications, especially when ML classifications had low confidence values.

GEOCHRONOLOGY

We analyzed zircons from twelve sites to determine U–Pb isotopic ratios using Laser Ablation Inductively Coupled Plasma Mass Spectrometry. These results assess provenance and maximum depositional ages (MDA) of sedimentary deposits, or eruptive ages of pyroclastic deposits. To do this, we sent approximately 7 kg of sample per site to ZirChron LLC for mineral separation. Zircon separates were analyzed by Vic Valencia and Jeff Vervoort at the Radiogenic Isotope and Geochronology Lab at WSU.

Detailed methods are in Appendix E and analytical data are available in the Data Supplement.

FLUXGATE MAGNETOMETRY

We used a portable fluxgate magnetometer to assess the polarity of whole rock magnetization—reverse or normal—for members of the CRBG at ~30 sites. This method is summarized in the appendix of Sadowski and others (2020). The technique is helpful for locating the changes between reverse and normal magnetization in the upper Grande Ronde Basalt and the upper Wanapum Basalt (units Mv_{wr} and Mv_{wp}). It is especially useful to distinguish Grouse Creek (reverse) and Ortley (normal) members of the Grande Ronde Basalt because they have similar elemental compositions.

DESCRIPTION OF MAP UNITS

Many of the units below—particularly Quaternary units and Grande Ronde units—are largely summarized from or are similar to descriptions of map units from Sadowski and others (2020, 2021, 2022).

Holocene to Pleistocene Nonglacial Deposits

- af **Artificial fill (Holocene)**—Cobbles, pebbles, sand, and boulders; poorly sorted and unconsolidated; includes foreign material placed to elevate home sites, highways such as I-90, I-82, and SR-821, railroads such as the BNSF track through Yakima Canyon, Palouse to Cascades State Park Trail, or other infrastructure. Notably, Canyon Rd/SR-821 and the BNSF railroad track were built on young alluvial deposits in Yakima Canyon. Unit af is at least 2 m thick.
- ml **Modified land (Holocene)**—Sand-through boulder-sized material, redistributed to modify topography for industrial, agricultural, recreational, and residential uses, including but not limited to gravel pits, rock quarries, aggregate mines, excavator training locations, and home sites. We mapped most of the town of Kittitas as modified land. Unit ml is at least 2 m thick.
- Qp **Peat (Holocene to Pleistocene)**—Organic and organic-rich sediment; includes peat, gyttja, muck, silt, and clay; typically in closed depressions; mapped in natural or man-made wetlands, bog areas, and ephemeral water bodies; also mapped from assessing black-and-white aerial photos where black to dark gray ephemeral ponds and water bodies are treated as peat. Smaller water bodies likely contain little to no peat deposits compared to larger older features. The thickness of most peat deposits is largely unassessed. Small peat deposits are scattered throughout the map area, typically within or near agricultural activities.
- Qls **Landslide deposits (Holocene to Pleistocene)**—Diamict; medium to light yellowish brown, weathering is typically mild or moderate; generally loose and poorly

consolidated; clay- to boulder-sized clasts; angular to subangular; poorly sorted, typically matrix supported; unstratified and structureless; unit **Qls** contains rubble of sand, silt, clay, cobbles, pebbles, boulders, and diamicton of mostly basalt clasts and with large quantities of silt and finer sands derived from nearby soils or sedimentary units (loess and volcanoclastic material); 5–60 m thick; unit **Qls** generally flanks uplands and steep canyons. Several large landslide complexes along the flanks of Manastash Ridge are near exposures of moderately dipping sedimentary interbeds—particularly units **MCev** and **MCelc**—and those sedimentary interbeds may have provided favorable slide planes for nearby landslides. Interstate 82—also known as US 97—goes through and near these large landslide complexes. Several south-facing hummocky landforms located north of Beavertail Bend contain only basalt float and form conspicuous topographic benches. We posit that these benches are related to sedimentary interbeds (unit **MCec**) and (or) ancient Yakima River strath terraces that would contain a diverse Cascade-sourced clast assemblage (unit **Qg**). Although we regularly found peperitic hyaloclastite related to the Coleman member, we could not find abundant and unambiguous evidence of non-basalt clasts at the surface. Unit **Qls** delineates confidently identified landslide deposits, whereas mass-wasting overlays delineate landforms with landslide-like characteristics (such as hummocky topography) that are difficult to characterize as landslide deposits. These overlays suggest places where evidence for landslide deposits is inconclusive and mass wasting may be related to other processes (such as soil creep and solifluction). Landslides and mass-wasting overlays are mapped primarily based on landform morphology. Absence of a mapped landslide or mass-wasting overlay does not indicate the absence of landslide hazard; site-specific investigations—and not this mapping alone—are recommended to further assess landslide hazards. We infer the age of unit **Qls** to be Holocene to Pleistocene, but recurrence is unknown.

Holocene to Pliocene Nonglacial Alluvial and Colluvial Deposits

Stream channel and stream flood (overbank) deposits and terraces. Deposits include pebbles, cobbles, sand, silt, clay, peat, and boulders, all in varying amounts and thicknesses. Colors range from light tannish gray to medium brown. Younger units are less compacted and cemented compared to older units. The clasts are typically pebbles and cobbles with sand and gravel, well rounded, moderately to well sorted, and mildly to moderately weathered. These units are generally composed of clasts of basalt (monomictic) away from the Yakima River corridor, whereas within the Yakima River corridor clast compositions are more diverse (polymictic) and contain abundant porphyritic andesite, dacite, other volcanic rocks, and some metamorphic rocks and trace quartz. We interpret these sediments near the Yakima River as being sourced mostly from the Cascade Range with minor contributions of dark-colored basalt, which we interpret

as being locally derived from nearby CRBG units. Numerous generations of alluvial and colluvial fans are exposed on the flanks of Manastash Ridge and the Boylston Mountains (see units **Qaf1**–**Qaf6**).

Qa Alluvium (Holocene)—Sand and gravel stream channel deposits on active flood plains; unit **Qa** is narrowly distributed throughout low elevations of the map area and these deposits commonly flank rivers and creeks; areas of this unit have been modified by infrastructure or agricultural cultivation. We infer the age of unit **Qa** to be Holocene and infer ongoing alluvial deposition on the surfaces of the unit.

Qia Intermediate-age alluvium (Holocene to Pleistocene)—Sand and gravel stream-flood (overbank) and old channel deposits near active flood plains where ongoing alluvial deposition from overland flow is possible; unit **Qia** is common in large portions of Kittitas Valley and along segments of Interstate 90; the Palouse to Cascades State Park Trail goes through this unit; surfaces of unit **Qia** are slightly elevated relative to the surfaces of unit **Qa**. Unit **Qia** likely contains significant amounts of silt derived from loess in the central portion of the Kittitas quadrangle. Material is poorly sorted silt to coarse sand with pebbles and rare cobbles. It is unclear where unit **Qia** ends and loess (overlay **Ql**) begins. We have chosen to map unit **Qia** to agree with mapping by Sadowski and others (2020, 2021). Unit **Qia** is challenging to distinguish from alluvial fan unit **Qaf1** based on their similar lithologies and heights relative to unit **Qa**. Unit **Qia** tends to be found closer to unit **Qa** than unit **Qaf1**, and units **Qia** and **Qaf1** are both above unit **Qa** surfaces, but unit **Qia** is at or slightly lower in elevation compared to unit **Qaf1**. We infer unit **Qia** to be slightly younger than **Qaf1** because of these slight elevation differences.

Qaf Alluvial fan and colluvial deposits (Holocene to Pliocene?)—Sand and gravel deposited in alluvial or colluvial fans and debris flow deposits; brown to medium gray; weathering rinds less than 1–10 mm thick; loose or poorly consolidated, but contains moderately to mildly cemented zones; silt- to boulder-sized clasts; angular to subrounded; poorly sorted; polymictic clasts are more common near the Yakima River; unit thickness is generally less than 15 m but older units may be thicker.

We subdivide this unit based on relative elevation above the modern stream level and differences in surface morphologies, and number the units from lowest and youngest (unit **Qaf1**) to highest and oldest (unit **Qaf6**). Older surfaces have smoother interfluvial surfaces and are more deeply incised, whereas younger surfaces are inset and rougher but less deeply incised; weathering rinds are <1 mm thick on unit **Qaf1**, about 1 mm thick on units **Qaf2** and **Qaf3**, and >1 mm thick on unit **Qaf4**. We also use a ~470 ka age on unit **Qaf3** from outside the map area (Sadowski and others, 2020) to anchor the relative ages in this map. Unit **Qaf1** may grade into unit **Qia** westward from Badger Pocket. Older surfaces of units **Qaf4**, **Qaf5**,

Table 1. Summary of ages. Additional details are in Appendix E and the Data Supplement. In the age column, '<' means 'no older than.' MDA stands for maximum depositional age.

Age site	Unit	Latitude (°N)	Longitude (°W)	Age ¹	Geochronological method	Age source
GD01	Mcev	46.97903	120.25918	< 48.93 ±1.89 Ma	zircon U-Pb (youngest single grain MDA)	This study
GD02	Mcev	46.94033	120.26902	< 16.25 ±0.40 Ma	zircon U-Pb (youngest single grain MDA)	This study
GD03	Mcev	46.95283	120.33518	< 15.96 ±0.048 Ma	zircon U-Pb (youngest population MDA)	This study
GD04	Mcev	46.97412	120.35458	< 15.90 ±0.09 Ma	zircon U-Pb (youngest population MDA)	This study
GD05	Mcev	46.98089	120.35697	15.95 ±0.08 Ma	zircon U-Pb (youngest population eruptive age)	This study
GD06	Mcelc	46.92310	120.33394	< 46.04 ±0.6 Ma	zircon U-Pb (youngest single grain MDA)	This study
GD07	Mcelc	46.88792	120.43247	< 14.82 ±0.36 Ma	zircon U-Pb (youngest single grain MDA)	This study
GD08	Mvce	46.90698	120.44955	< 10.38 ±0.35 Ma	zircon U-Pb (youngest single grain MDA)	This study
GD09	Mvce	46.92198	120.46544	8.72 ±0.04 Ma	zircon U-Pb (youngest population eruptive age)	This study
GD10	Mcge	46.94232	120.49481	< 5.41 ±0.14 Ma	zircon U-Pb (youngest single grain MDA)	This study
GD11	Mcge	46.88034	120.32488	< 5.22 ±0.78 Ma	zircon U-Pb (youngest single grain MDA)	This study
GD12	Rcg	46.99100	120.39696	< 3.26 ±0.18 Ma	zircon U-Pb (youngest single grain MDA)	This study
GD13	Rcg	46.94222	120.49472	2.9 ±0.1 Ma	quartz ²⁶ Al– ¹⁰ Be (cosmogenic burial age)	Bender and others (2016)
GD14	Qg	46.90940	120.49750	1.0 ±0.2 Ma	quartz ²⁶ Al– ¹⁰ Be (cosmogenic burial age)	Bender and others (2016)
GD15	Qg	46.89990	120.49389	88.75 ±4.52 ka	K-feldspar (from loess) IRSL	Age from Ladinsky (2012), location reported in Bender and others (2016)

¹ Uncertainties are 2σ except for those for GD13, GD14, and GD15, which are 1σ.

and Qaf6 commonly have loess, fault escarpments, and hardpan of calcrete and (or) silcrete. For these three units, we extrapolated mapping by Kelsey and others (2017) and suspect portions of unit Mcge along Manastash Ridge may be unit Qaf6 or unit Qaf5 based on their similar clastic lithologies. Based on map patterns, we infer gently north-dipping contacts between these older units near Manastash Ridge. Multiple similarly-aged, closely-spaced, fan-shaped deposits of unit Qaf4 are along the southwestern flank of the Boylston Mountains (see 'Geologic boundary' symbols in the map legend) and onlap onto upper Ellensburg Formation unit Mcge. Near Wippel Creek, unit Qaf4 consists of sediment eroded from the Boylston Mountains and its basaltic clasts are mildly to moderately cemented along the southwestern mountain flank. We see similar cementation on other Pliocene units. Without age control, we wonder if portions of units Qaf4, Qaf5, and Qaf6 are older than we depict on our *Correlation of Map Units* (see Map Sheet).

Qg Terrace gravel deposits (Pleistocene)—Gravel deposited in fluvial setting in Yakima Canyon; light to medium gray, greenish gray, light to medium brown; loose,

poorly cemented; pebbles and cobbles with boulders and medium sand; rounded to subrounded; poorly sorted, matrix supported; polycrystic clasts include Cascades-sourced andesite and sparse metamorphic rock with locally sourced basalt; unit Qg thickness is at least several meters thick (~5 m); located in Yakima Canyon to the north of State Route 821. Unit Qg directly overlies CRBG units and underlies loess (overlay Ql) and young fan deposits (unit Qaf2). We interpret unit Qg as strath terrace deposits from the paleo-Yakima River. These deposits are elevated above the valley floor (>50 m) suggesting that they were uplifted possibly by deformation related to Manastash Ridge. A cosmogenic nuclide ²⁶Al–¹⁰Be isochron burial age is 1.0 ±0.2 Ma (age site GD14) (Bender and others, 2016). Queried Qg map unit polygons near age site GD14 are possibly older strath terrace deposits or gravels from the upper Ellensburg Formation.

Rcg

Cobble gravel (Pliocene)—Cobble gravel with sandy interbeds; medium brown; deposits form broad, elevated, smooth yet deeply incised amorphous fan-like landforms; unit Rcg is strongly weathered with basalt clasts having weathering rinds greater than 1 mm

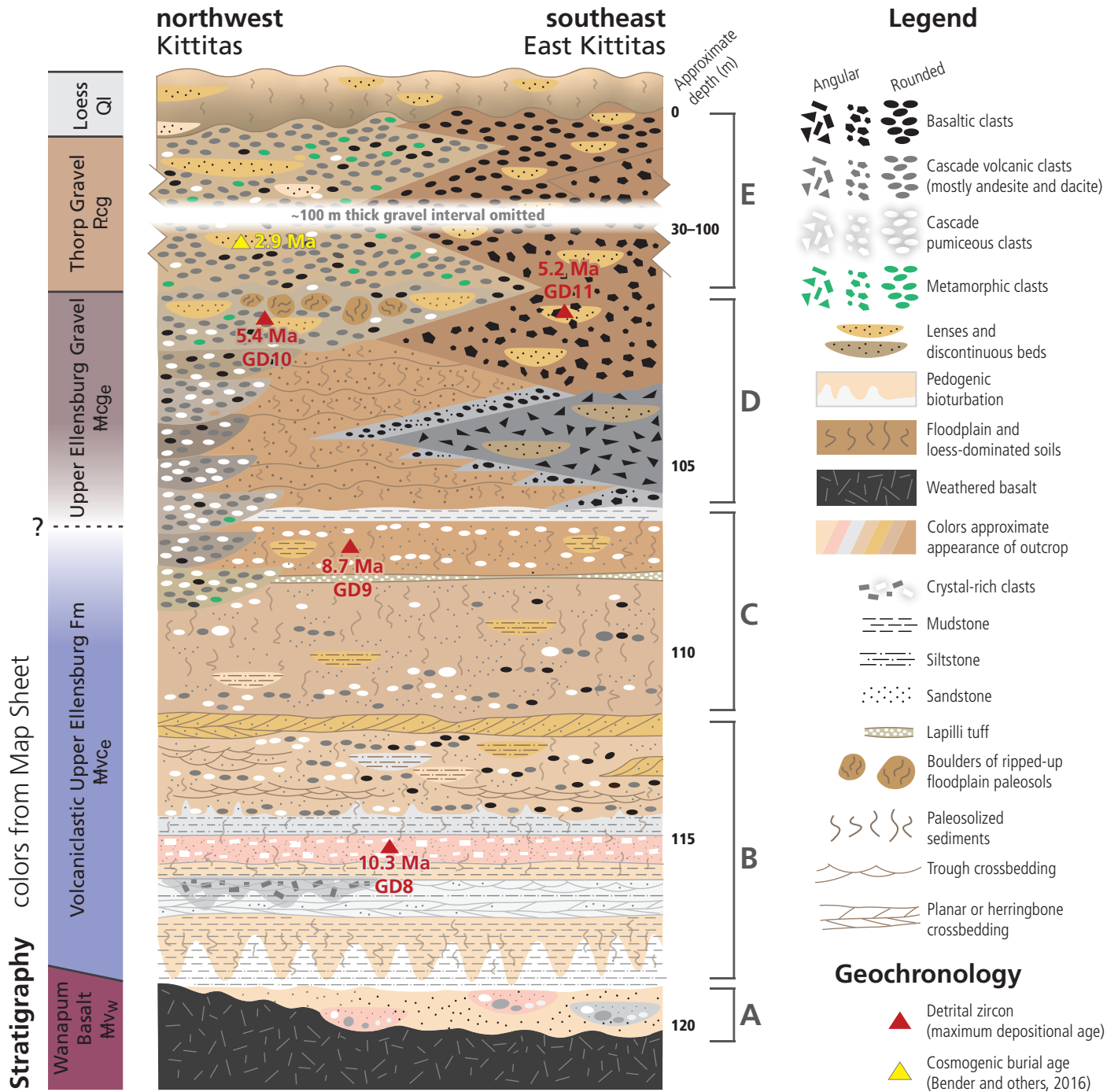


Figure 2. Interpretative composite stratigraphic section summarizing observed lithologic trends in outcrops of late Miocene suprabasalt upper Ellensburg Formation between the northern flank of Manastash Ridge and Kittitas Valley. The Ellensburg Formation is better exposed in the Kittitas quadrangle than in the East Kittitas quadrangle. Material overlying the Ellensburg Formation is well exposed in both quadrangles. This figure is based on observations from numerous outcrops and includes significant lateral and vertical interpolation to connect isolated observations.

thick; moderately to mildly cemented, moderately indurated; deposits contain cobbles and pebbles with fine- to coarse-grained sand; angular to subrounded; moderately to poorly sorted, clast supported; near the Yakima River, this unit is polymictic but with a high proportion of CRBG clasts; elsewhere it typically contains just CRBG clasts. In sandy interbeds, cobbly volcaniclastic material in a fine matrix suggests that some interbeds may be distal portions of lahars. Unit

Rcg is at least 2 m thick near Potato Hill (location on Fig. 1) (upper portions of E on Fig. 2), over 30 m thick near Johnson Canyon, and may be far thicker (>100 m?) at depth in Kittitas Valley based on well data. Unit Rcg is common on the flanks of the Boylston Mountains, especially where the unit's westward fanning deposits emerge from Johnson Canyon and Wippel Creek. Unit Rcg onlaps onto unit McGe at Potato Hill.

We obtain a U-Pb maximum depositional age (MDA) of 3.26 ± 0.18 Ma (GD12) from a laharic sandstone lens, which is similar to and likely age correlative with the Thorp Gravel (Waite, 1979). Age spectra from unit Rcg (age site GD12) contains a single Proterozoic detrital zircon grain, its only pre-Cenozoic zircon. This dearth of older detrital zircons suggest that this unit has a different provenance from other older sedimentary units, such as the Ellensburg Formation in Kittitas Valley, which contain plentiful pre-Cenozoic zircons.

We can bracket the beginning of unit Rcg sedimentation to after ~ 5.4 Ma (age site GD10) and before ~ 4.15 Ma based on a U-Pb age from the Indian Trail Ash at Craigs Hill within the Thorp Gravel (Fields, 2023). Our bracketing is supported by a cosmogenic nuclide ^{26}Al – ^{10}Be isochron burial age of 2.9 ± 0.1 Ma (geochronology site GD13) (Bender and others, 2016) near the base of unit Rcg at Potato Hill.

Tertiary Sedimentary and Volcanic Bedrock

SEDIMENTARY ROCKS OF THE ELLENSBURG FORMATION

We map several different members of the Ellensburg Formation based on their lithology and stratigraphic relationship with flows of the CRBG. Those sedimentary units that are intercalated with the CRBG include units M_{Cec} , M_{Cev} , and M_{Celc} . We refer to these informally as the lower Ellensburg Formation or Ellensburg interbeds. These units are typically micaceous to tuffaceous sandstone to siltstone, 35 m thick or less, and not well exposed. Sedimentary units that overlie the CRBG include volcanoclastic and conglomeratic units (M_{Vce} and M_{Cge} respectively). Within the map area, we refer to these informally and locally as the upper Ellensburg Formation or suprabasalt Ellensburg units. It is possible that correlative upper Ellensburg units may be interbedded with CRBG elsewhere in the Columbia basin where younger CRBG units erupted (for example, the Saddle Mountains Basalt) and capped volcanoclastic and (or) conglomeratic Ellensburg lithologies. Compared to the lower units, the upper Ellensburg units have greater lithologic variability, greater amounts of coarser material and calcrete–silcrete, more volcanoclastic material, and are much thicker (120 m thick or more) and less tilted. Lower Ellensburg units also have consistently greater amounts of pre-Cenozoic zircons compared to upper Ellensburg units (Data Supplement). Figure 2 summarizes the lithostratigraphy of the upper Ellensburg Formation, which unconformably overlies and onlaps Wanapum Basalt (unit M_{Vw}). We interpret Ellensburg Formation rocks to have fluvial, lacustrine, volcanoclastic, and colluvial origins. At depth in Kittitas Valley, Ellensburg Formation units may form aquifers or aquitards depending on their ash content (because ash weathers to clay). When the formation forms an aquitard, groundwater resources can be perched in overlying lithologies.

M_{Ce} Ellensburg Formation, undivided (middle Miocene to early Pliocene?)—Feldsarenite, volcanoclastic sandstone, and conglomerate; light to medium brown or light to medium gray; mildly to strongly weathered; moderately indurated; subrounded or subangular; well to

moderately sorted; grain supported; composition of sand is quartz (20–35%), feldspar (plagioclase 10–20%, potassium feldspar 5–15%), and lithic fragments (3–10%), with varying abundances of muscovite (0–30%).

We map undivided unit M_{Ce} where we lack grain size observations especially at depth and infer a local suprabasalt stratigraphic position (i.e. upper Ellensburg Formation) within the map area. Based on lithology and stratigraphic position relative to CRBG units, we locally subdivided the Ellensburg Formation into:

M_{Cge} Conglomeratic rocks of the upper Ellensburg Formation (late Miocene)—Gravelly conglomerate with lenses of siltstone to sandstone; light brownish gray to medium brown, mild to moderately weathered; mild to moderately cemented; pebbly cobble gravel with few boulders and coarse to fine sand; subangular to well rounded; poorly sorted, matrix supported; structureless to uncommonly very thickly bedded with alternating laminated fine sandstone and siltstone. Near the Yakima River and Manastash range front, the bottom of unit M_{Cge} contains dacite (50%), andesite (30%), and rhyolite (20%) with some locally derived gravels of CRBG clasts, and trace pumice and quartz. The upper section of the unit adds the following to the aforementioned assortment: some metamorphic (\pm intrusive?) clasts from the Western Mélange Belt (Fig. 2D), an early Mesozoic relict accretionary prism exposed west of the map area along the western Cascade Range. Near the Yakima River at Potato Hill, we found boulder-sized rip up clasts composed of laminated sandstones that are volcanoclastic, tuffaceous, and (or) basaltic (northwest side of D on Fig. 2). Away from the Yakima River, clast compositions are monomictic basalt likely entirely from nearby CRBG units (southeast side of D and E on Fig. 2). The amount of cementation near both areas is similar to unit Rcg. Away from the Yakima River, we wonder if we misidentified portions of unit M_{Cge} and portions of map unit polygons could instead be younger colluvium—units Qaf_5 or Qaf_6 —based on their similar appearances and a lack of more detailed age control. Unit M_{Cge} is at least 100 m thick. Unit M_{Cge} is diagnostically more conglomeratic and less volcanoclastic than underlying unit M_{Vce} . Lower contact with unit M_{Vce} was not observed and may be associated with a marked decrease in dacite and pumice content or otherwise gradational with unit M_{Vce} (upper part of C on Fig. 2). U-Pb analyses of detrital zircons from unit M_{Cge} yield maximum depositional ages (MDAs) of $\leq 5.22 \pm 0.78$ Ma (age site GD11) in Badger Pocket and $\leq 5.41 \pm 0.14$ Ma (age site GD10) at Potato Hill. MDAs from units M_{Cge} and Rcg

suggest that deposition of the upper Ellensburg Formation may have ceased between ~5.4 Ma (age site GD10) and ~3.3 Ma (age site GD12), likely close to the Miocene–Pliocene boundary. The upper part of this unit may be as young as Pliocene (Schmincke, 1967b).

Mvce Volcaniclastic rocks of the upper Ellensburg Formation (late Miocene)—Volcaniclastic sandstone, siltstone, and mudstone with some conglomerate; light to medium gray, pinkish brown, light brown, or light orangish brown; moderately weathered; moderately indurated to friable, mild to moderately cemented; lithology varies from fine- to coarse-grained tuffaceous sandstone, siltstone, and mudstone; thin lamina of ash fall tuff and accretionary lapilli tuff; and loess-rich paleosol intermingled throughout; subangular to rounded; poorly sorted, matrix supported; some lithologies commonly show trough and planar crossbedding in lower sections. Sand compositions include abundant pumice (usually rounded, less commonly angular), porphyritic hornblende-rich dacite (common throughout and diagnostic of unit **Mvce**), loess, and (or) rounded clasts of local basalt and Cascade-sourced dacite with greater andesite. We broadly infer that the dacite clasts are from the Cascade Range but are unsure of the exact source(s) and age(s) of those clasts. Unit **Mvce** is at least ~20 m thick and may grade into overlying unit **Mcge**. Unit **Mvce** is diagnostically more volcaniclastic and less conglomeratic than overlying unit **Mcge**. Unit **Mvce** overlies the Priest Rapids Member (unit **Mvwp**) and underlies no other basalt in the map area. Based on its lithology and stratigraphic position above unit **Mvwp**, unit **Mvce** is probably correlative, at least in part, to the Selah member (Smith, 1988a,b; Bingham and Grolier, 1966) or more formally the Beverly Member (Mackin, 1961; Bingham and Grolier, 1966; Reidel and others, 2013a). Unit **Mvce** may also be part of the Mabton member (Mackin, 1961; Smith, 1988a), which overlaps with the Selah and Beverly members. Outside the map area, these named members are regional interbeds of the Saddle Mountains Basalt (for example, the lower Ellensburg Formation on the northern flank of the Saddle Mountains ridgeline). However, the correlative unit **Mvce** is locally in a suprabasalt position within the map area. In other words, unit **Mvce** is locally an upper Ellensburg unit, and regionally a lower Ellensburg interbed. U-Pb analysis of a pumice separate directly above an accretionary lapilli tuff marker bed near the transition from unit **Mvce** to **Mcge**

(Fig. 2) yields an age of 8.72 ± 0.04 Ma (age site GD09), which we interpret as an eruptive age. An additional U-Pb analysis of a pumiceous sandstone closer to the base of the unit yields a maximum depositional age of $\leq 10.38 \pm 0.35$ Ma (age site GD08).

Mcclc Lmuma Creek Member of the lower Ellensburg Formation (middle Miocene)—Tuffaceous—and less commonly basaltic—sandstone and locally diatomaceous siltstone; light gray to white, mildly to moderately weathered; mildly indurated or friable, mildly to moderately cemented; medium grained; subrounded; well sorted, matrix supported; commonly shows planar crossbedding that is somewhat diagnostic; rare polymictic pebble layers; sand composition includes abundant ash and basalt fragments; diagnostically has varied amounts of diatomite and less muscovite than unit **Mcce**; less than 15 m thick. At the base of the unit, we observe a thin diatomite lens (<10 cm thick) on the south limb of the Vanderbilt Gap syncline. This lens contains diatoms of genera *Melosira* and *Odontidium* (I. Hong, written commun., Villanova University, 2023), both of which are freshwater varieties. Based on lithologies, map patterns, and these diatoms, we interpret sediment of unit **Mcclc** was likely deposited in a freshwater fluvial-lacustrine paleoenvironment above the Frenchman Springs Member (unit **Mvwfsh**). Based on peperitic hyaloclastite and field relationships near Vanderbilt Gap, we hypothesize these sediments were later invaded by Roza Member lavas (unit **Mvwr**), where unit **Mcclc** is typically below and sometimes above the Roza Member. Unit **Mcclc** is tilted and folded. We infer a paleocurrent (from north to south) based on sandy tuffaceous crossbeds at age site GD07. Also at age site GD07, our ~14.8 Ma MDA appears to be too young based on a high-precision ID-TIMS age of 15.895 ± 0.019 Ma from an ash in the overlying Priest Rapids Member farther east (Kasbohm and Schoene, 2018). From unit **Mcclc**, age site GD06 shows pre-Cenozoic zircons in greater abundances than in age site GD07. We interpret these differences in U-Pb age spectra as a westward change in sediment sourcing, where eastern areas received greater amounts of older zircons than western areas.

Unit **Mcclc** was formerly divided from the Quincy diatomite that overlies the Roza Member outside the map area, but now the Lmuma Creek Member may include that

diatomite. We use this unit for sedimentary rocks above unit **Mv_{wfsh}** and below unit **Mv_{wp}**.

Formerly known by a term derogatory to Indigenous women, our report formalizes the renaming of this unit as per U.S. Department of the Interior Secretarial Orders 3404 and 3405.

M_{Cev} Vantage Member of the lower Ellensburg Formation (middle Miocene)—Micaceous sandstone and siltstone, and volcanoclastic deposits; light brownish gray to light gray or white-yellowish tan; moderately to strongly weathered; mildly to moderately indurated, mildly cemented, low density; subangular to subrounded; fine to coarse grained, and commonly medium grained; commonly well sorted, grain supported; sand composition is variable (feldspathic or siliciclastic dominant), compared to unit **M_{Celc}**, unit **M_{Cev}** has more quartz, more muscovite, and less basaltic fragments. A local composite section of unit **M_{Cev}** based on field relationships shows four parts: (1) a basal micaceous sandstone to siltstone (1–3 m thick) with common orange–brown lie-segang banding; (2) an opaque, brownish-gray vitreous or resinous layer (5–25 cm thick, ash?) that is fractured and weathered; (3) couplets of fine- over coarse-grained volcanoclastic sandstone (as many as ~14 pairs, <2 m thick per pair) that represent multiple rapid catastrophic events, possibly distal lahars, deposited into a lacustrine setting; and (4) an uppermost hornblende-rich ash fall tuff (<1 m thick) that is unwelded, contains no fiamme, and may have been heated by subsequent lavas of the Wanapum Basalt. Unit thickness is ~30 m near Yakima Canyon and Vanderbilt Gap, and less than ~20 m thick elsewhere. Unit **M_{Cev}** is more common in our map area compared to northward adjacent map areas (Sadowski and others, 2022), which may suggest a local change in depositional center. Sedimentation of unit **M_{Cev}** represents a local pause in CRBG eruptions. Based on fine-grained lithologies, we interpret a low-energy fluvial(?)–lacustrine depositional environment.

In a basalt quarry, a Miocene petrified red oak (*Quercus sahnii*, Prakash and Barghoorn, 1961a,b) stump in growth position is rooted in unit **M_{Cev}** with pillows of Wanapum Basalt surrounding the trunk (J. Landon, written commun., 2021). Unit **M_{Cev}** unconformably overlies Grande Ronde Basalt unit **Mv_{gsm}** and underlies Wanapum Basalt unit **Mv_{wfsh}**, less so unit **Mv_{wfg}**. We collected geochronology samples at five sites (GD01–05, Table E1). U-Pb analysis of zircons from a contact metamorphosed(?) tuff near the top of the Vantage Member yields an age of 15.95 ± 0.08 Ma (age

site GD05). We interpret this as an eruptive age for the tuff that is compatible with a U-Pb ID-TIMS analysis of a pumice separate (sample CRB1533, 16.066 ± 0.040 Ma) by Kasbohm and Schone (2018) near Vantage, WA (~28 km east of age site GD05). Age spectra from Vantage Member age sites GD01 and GD02 contain abundant pre-Cenozoic zircons, whereas age sites GD03–05 lack abundant pre-Cenozoic zircons. We infer that this lack of older zircons is from a lack of sediment supplying older zircons to age sites GD03–05. Based on the lacustrine paleoenvironment and the lack of older zircons, we suspect the existence of a middle Miocene paleolake in the ancient area where the Boylston Mountains would form (or were forming). This area encompasses age sites GD03–05 but not GD01 nor GD02.

M_{Cec} Coleman member of the lower Ellensburg Formation (middle Miocene)—Sandstone and siltstone underlying the Winter Water Member and overlying the Grouse Creek member; medium brown to light gray; variably micaceous; fine- to medium-grained sandstone. Unit **M_{Cec}** is discontinuous and poorly exposed at mid elevations in Yakima Canyon. We estimate it to be less than 20 m thick, probably much thinner and pinching out eastward based on map patterns. This may suggest that the Coleman member's depositional center is farther west or north outside the map area. Its depositional environment is likely a Miocene fluvial and (or) lacustrine setting (Sadowski and others, 2020, 2021). We map a discontinuous outcrop pattern of isolated lenses encompassed by Ortley basalt (unit **Mv_{go}**) in Yakima Canyon north of Beavertail bend, and infer that these lenses are unit **M_{Cec}** based on stratigraphic position and lithology. Hyaloclastites associated with GRB flows near unit **M_{Cec}** are less common in the map area compared to other quadrangles to the north. Unit **M_{Cec}** is more common than unit **M_{Cev}** northwest of the map area, and unit **M_{Cev}** is more common than **M_{Cec}** within the map area. On this basis, and given that unit **M_{Cec}** is older than unit **M_{Cev}**, we interpret that the depositional center may have migrated from the northwest to the south or east during the middle Miocene. Landslides are common downslope of unit **M_{Cec}** because the unit appears to easily form slide planes for mass wasting.

The unit was informally named by Bentley (1977) near Coleman Canyon of northern Kittitas Valley and mapped by Hammond (2013) as far south as the Naches River area. It is equivalent to the farther north Rock Island member of Hoyt (1961), the Douglas Creek

member of Ebinghaus and others (2015), and the Rock Island arkosic sand of Schmincke (1967a). We do not map subdivisions of this unit because available exposures in the map area proved insufficient for recognition of grain size subdivisions (similar to those reported outside the map area by Sadowski and others, 2020, 2021).

VOLCANIC ROCKS OF THE COLUMBIA RIVER BASALT GROUP (CRBG)

Flood basalts of the Columbia River Basalt Group (CRBG) are well documented in volumes by Reidel and Hooper (1989) and Reidel and others (2013c). We follow stratigraphic nomenclature from these volumes and list previously used nomenclature from unpublished maps near the end of the unit descriptions in this pamphlet. We map members and submembers of the Grande Ronde Basalt (GRB) and Wanapum Basalt of the CRBG.

Mv_w Wanapum Basalt, undivided (middle Miocene) (cross section only)—Porphyritic and aphyric basalt to basaltic andesite, described in detail in the following subunits; dark gray to grayish brown; dense; mostly microporphyritic to weakly glomerocrystic, commonly with groundmass crystals larger than 1.0 mm and less commonly aphyric than GRB units; groundmass textures are microcrystalline, equigranular to seriate, and plagioclase microlite laths are unoriented (pilotaxitic more than trachytic); compared to GRB units, thin sections of Wanapum Basalt units show more weathering and common silica infilling (opal-AG) of microscopic voids. In the map area we infer the presence of the unit where moderate-relief landforms are found stratigraphically above unit **Mc_{ev}**. The unit unconformably overlies the Vantage Member (unit **Mc_{ev}**), and upper Ellensburg Formation units onlap this unit. At Vanderbilt Gap, the Frenchman Springs and Roza members have a combined thickness of ~85 m with an additional ~15 m of Priest Rapids Member for a total thickness of ~100 m. Overall, this unit and its subunits are generally thinner than the more voluminous GRB (unit **Mv_g**). Sedimentary interbeds are more common in the Wanapum Basalt subunits than in the GRB. Undivided unit **Mv_w** groups Wanapum Basalt subunits at depth in the cross section. We classify Wanapum Basalt subunits with geochemical data and they include:

Mv_{wp} Priest Rapids Member (middle Miocene)—Medium- or very coarse-grained basalt and basaltic andesite with groundmass crystals ranging in size from 0.5 to 2 mm; dark gray to grayish brown, can weather to light orangish brown; dense; mostly aphyric to weakly porphyritic, otherwise characteristically coarse-grained, and less commonly very coarse-grained as a basaltic pegmatoid (gabbroic texture); dense; based on elevated TiO₂ (>3.3 wt.%) this unit is likely the basalt of Rosalia, a reverse polarity flow set within

the lower Priest Rapids Member; ~15 m thick as estimated from Vanderbilt Gap, and may be thicker north and down from the ridgeline, where the top is less well exposed. The unit may thicken into Kittitas Valley based on geophysical modeling. Unit **Mv_{wp}** generally directly overlies the sedimentary Lmuma Creek Member (unit **Mc_{elc}**), if present above the Roza Member, otherwise unit **Mv_{wp}** overlies the Roza Member. Unit **Mv_{wp}** is the uppermost member of the Wanapum Basalt and the youngest basalt in the map area.

Mv_{wr} Roza Member (middle Miocene)—Porphyritic basalt and basaltic andesite with a medium to fine groundmass; dark gray to grayish brown, weathers dark to medium brown; dense; diagnostically porphyritic with common centimeter-scale (4–14 mm) phenocrysts (total phenocrysts: 5–10%, mostly plagioclase), generally contains about a dozen phenocrysts (more than about 10) per hand sample, but top of unit **Mv_{wr}** can be more aphyric; several Roza compositional types exist and we map only Roza compositional unit Type IIA (Martin, 1989); ~15–30 m thick; middle and especially high elevations on Manastash Ridge have good exposures of unit **Mv_{wr}**, whereas near the mouth of Wippel Creek exposures of unit **Mv_{wr}** were limited to float. The unit also pinches out on the northern flank of the Boylston Mountains. Unit **Mv_{wr}** typically overlies the sedimentary Lmuma Creek Member (unit **Mc_{elc}**) and thin portions of unit **Mc_{elc}** can also overlie the Roza Member. Pillow breccia mixed with sedimentary material (unit **Mc_{elc}**) is very common in the Roza Member in the map area, which we interpret as peperitic hyaloclastite. This lithologic observation and nearby field relationships strongly suggest that Roza lavas invaded sediments of the Lmuma Creek Member. Unit **Mv_{wr}** has a ⁴⁰Ar/³⁹Ar eruption age of 14.98 ± 0.17 Ma (Barry and others, 2013). Unit **Mv_{wr}** has transitional or excursions magnetic polarity. Unpublished mapping by Bentley and Powell in the early 1980s labels this unit as “Tr”. Reference locality for unit is at the I-82 southbound overlook located north and upsection from age site GD07.

Mv_{wf} Frenchman Springs Member, undivided (middle Miocene)—Medium-grained basalt to basaltic andesite that is sparsely porphyritic to weakly glomerocrystic or aphyric, described in detail in the following subunits; dark gray to grayish brown; dense; commonly sparsely porphyritic to glomerocrystic with less than 3 percent total phenocrysts (mostly plagioclase)

to aphyric; unit is less than 90 m thick with Ginkgo and Sand Hollow units combined, and thickness may increase at depth in Kittitas Valley. In the map area, the Frenchman Springs Member is less porphyritic than the Roza Member and finer grained than the Priest Rapids Member. Frenchman Springs subunits generally have normal magnetic remanence, but can be transitional or excursions near its base. Unit **M_{Vwf}** is mapped as undivided and typically inferred wherever geochemistry was unavailable to divide exposures into subunits or inferring a particular subunit was overly speculative, or at depth in cross section.

M_{Vwfs} Basalt of Sand Hollow (middle Miocene)—Medium-grained basalt and basaltic andesite that is weakly porphyritic to aphyric; medium to dark gray, weathers to dark reddish brown or reddish gray; dense; typically contains a few 1–15-mm-long euhedral phenocrysts (usually about two) per hand sample (total phenocrysts: ~1%), some of which may be glomerocrysts; ~1-m-wide columns can internally exhibit flat to curved platy foliation; pillow breccias and palagonite (hyaloclastite) are also common. Unit is generally ~40 m thick and rarely thicker than 60 m. Unit **M_{Vwfs}** forms good outcrop exposures and is widespread but less well exposed where it caps small hills in the northern map area. Unit **M_{Vwfs}** is common on the north flank of the Boylston Mountains, near the mouth of Wippel Creek, near Park Creek, spread throughout the northern map area, and in the upper elevations of Manastash Ridge. Many rock quarries in the northern half of the East Kittitas quadrangle are mining this unit for aggregate. Where basalt of Ginkgo (unit **M_{Vwf}**) is absent, unit **M_{Vwfs}** can directly overlie the Vantage Member (unit **M_{Cev}**) and directly underlie the sedimentary Lnuma Creek Member (unit **M_{Celc}**). Unit **M_{Vwfs}** has an ⁴⁰Ar/³⁹Ar plateau age of 15.12 ± 0.38 Ma (Barry and others, 2013). This unit was previously known as the “Kelley Hollow flow” and sometimes referred to as the “Double Barrel flow.” Unpublished mapping by Bentley and Powell in the early 1980s labels this unit as **Tfk** (Frenchman Springs Kelley Hollow) or **Tkh** (Kelley Hollow). Note

that prior usage of the name “Sand Hollow flow” (Bentley, 1977) referred to the aphyric variety of the middle Frenchman Springs Member that underlies the “Kelley Hollow flow.” “Kelley Hollow” and “Sand Hollow” units were originally split based on phenocryst content, and flow units are now grouped based on having similar geochemical compositions (Martin and others, 2013).

M_{Vwfg} Basalt of Ginkgo (middle Miocene)—Medium-grained basalt that is weakly porphyritic or glomerocrystic; medium to dark gray, weathers to medium or dark brown; dense; typically contains less than a half dozen phenocrysts generally four per hand sample (total phenocrysts: 1–2%), some of which may be glomerocrysts; ~30 m thick and pinches out westward toward Badger Pocket; rarely forms good exposures and is only common at mid elevations of the Boylston Mountains; typically overlies the Vantage Member (unit **M_{Cev}**) and directly underlies the basalt of Sand Hollow (unit **M_{Vwfs}**); named for abundant petrified trees ~20 km east of the map at Ginkgo Petrified Forest State Park near Vantage, Washington.

M_{Vg} Grande Ronde Basalt (GRB), undivided (middle Miocene) (cross section only)—Basaltic andesite, described in detail in the following subunits and briefly summarized here. Generally, GRB rocks in hand specimen are very dark to medium gray where fresh, dark to medium brown where weathered, and dense; in thin section they show euhedral laths of plagioclase microlites (<1 mm in size) intermeshed in an irregular and unoriented microcrystalline groundmass texture (pilotaxitic or felty).

GRB members are categorized into four polarity chronostratigraphic units, also known as magnetostratigraphic units (MSU). These magnetostratigraphic units of the GRB are from oldest to youngest: reverse magnetic polarity 1 (R1 MSU), normal magnetic polarity 1 (N1 MSU), reverse magnetic polarity 2 (R2 MSU), and normal magnetic polarity 2 (N2 MSU) (Tabor and others, 1982; Reidel and Tolan, 2013; Hammond, 2013). In the map area, R1 and N1 MSU have not been observed and we subdivide R2 and N2 MSU further into chemostratigraphic subunits where geochemistry data is available (Data Supplement). Unit **M_{Vg}** is inferred where geochemistry was unavailable, outcrops were absent, inference for a particular subunit was overly speculative, or units were grouped at depth in cross section (for

example, portions of Grouse Creek (R2 MSU) and older GRB units are grouped at depth).

Without the base exposed, we map a minimum GRB thickness of at least ~400 m. From the Shell BISSA 1-29 borehole we estimate a thickness of ~4,600 ft (~1,400 m) of basalt that we interpret to be all GRB, assuming no faulting through the borehole (Wilson and others, 2008; Czajkowski and others, 2012). However, there may be a fault downhole through the Wapshilla Ridge Member (part of the R2 MSU; S. Reidel, WSU Tri-Cities, written commun., 2020). The 23-35 BN Meridian Oil, Inc well is <1.5 km from cross section B and has ~6,658 ft (2,029 m) of basalt (Czajkowski and others, 2012). Notably, it has a very thick (>750 m) R1 MSU. Downhole geochemical sampling intervals of the basalts are not as closely spaced as the BISSA well so thickness measurements from the Meridian well are less constrained and should be considered approximate (S. Reidel, WSU Tri-Cities, written commun., 2020).

Mvgs Sentinel Bluffs Member, undivided (middle Miocene)—Basaltic andesite; aphyric; the uppermost member of the Grande Ronde Basalt; the map area contains five subunits, from oldest to youngest: basalts of McCoy Canyon, California Creek, Spokane Falls, Stember Creek, and Museum, where the middle three subunits are portions of the Cohasset flow (Reidel, 2005) that may be intermingling compositional types and may locally exhibit an internal vesicular zone (IVZ) related to flow inflation (McMillan and others, 1989; Reidel, 2015). Member and subunits have normal magnetic polarities (N2 MSU). Undivided **Mvgs** is used in the cross section to group its subunits at depth. Where present, the IVZ may obscure the locations of vesicular flow tops identified from surface mapping of physical volcanology characteristics, because vesicular flow tops and the IVZ look similar. Where geochemical results are available (Data Supplement), we use cross comparisons of geochemical variation diagrams (TiO₂ vs. MgO, TiO₂ vs. P₂O₅, Zr, and Cr, for example) and stratigraphic relationships to classify flows geochemically. This is especially useful where elemental compositional fields partially overlap for the middle-to-upper subunits on TiO₂ vs. MgO diagrams but not necessarily on TiO₂ vs. P₂O₅ diagrams. Cumulatively, the Sentinel Bluffs Member is at least ~140 m thick, and its sub-units are common throughout the map area. The Meridian well has an approximate thickness for the Sentinel Bluffs Member of 93–125 m (S. Reidel, WSU Tri-Cities, written commun., 2020). The unit was previously mapped as GRB N2 MSU (Tabor and others, 1982). Unit **Mvgs** is mapped as undivided where geochemical results are unavailable to

divide exposures into subunits but where we remain reasonably confident that the exposure belongs to the Sentinel Bluffs Member based on interpolations with nearby stratigraphic relationships. The geochemical compositional ranges of all subunits of unit **Mvgs**—that is the elemental composition of the Sentinel Bluffs Member as a whole—generally are: TiO₂: ~1.7–2.0 wt. %, MgO: ~3.8–5.5 wt. %, P₂O₅: ~0.26–0.39 wt. %, Zr: ~145–174 ppm. Using whole-rock geochemistry (Data Supplement), we subdivide the Sentinel Bluffs Member into:

Mvgsm Basalt of Museum (middle Miocene)—Fine-grained basaltic andesite with groundmass crystals ranging in size from 0.05 to 0.6 mm and very rare phenocrysts of plagioclase up to 3.5 mm in size; most commonly aphyric; groundmass textures are micro-crystalline, mostly equigranular (rarely seriate), and pilotaxitic (unoriented). Museum compositions are very similar to Spokane Falls compositions locally. Other contents include mafic minerals (20–40%, 0.1–0.5 mm, mostly clinopyroxene) and devitrified glass that is absent or rare. From map patterns, unit thickness is ~38–60 m in Yakima Canyon to at least ~87 m near Vanderbilt Gap. Unit is commonly mined for aggregate in the map area and Kittitas Valley. The upper contact is poorly exposed. At depth, unit thickness in the BISSA well is ~60 m (S. Reidel, WSU Tri-Cities, written commun., 2020). Unit contains at least one flow with colonnades, entablatures, and vesicular tops that are all well developed. Unit is widespread and found along the higher portions of Manastash Ridge and throughout the Boylston Mountains. Unpublished mapping by Bentley and Powell in the early 1980s labels this unit as Tmz (Museum), Tor (Ortley Rocky Coulee), or Trc (Rocky Coulee), but recent refinement of GRB stratigraphy (Reidel, 2005; Reidel and Tolan, 2013) lumped these compositional types together as the basalt of Museum, which we adhere to.

Mvgssc Basalt of Stember Creek (middle Miocene)—Fine-grained basaltic andesite with groundmass crystals ranging in size from 0.05 to 0.4 mm and very rare phenocrysts

of plagioclase as large as 1.6 mm; most commonly aphyric; groundmass textures are microcrystalline, seriate more than equigranular, and pilotaxitic (unoriented). Unit **Mvgssc** generally has diagnostically lower zirconium values compared to other sub-units of the Sentinel Bluffs Member. Higher chromium and lower zirconium values are particularly effective for distinguishing unit **Mvgssc** from unit **Mvgssf**, especially where stratigraphic relationships are less straightforward. Other contents include mafic minerals (<30%, 0.05–0.35 mm, mostly clinopyroxene) and some devitrified glass (0–15%). From map patterns, the unit is less than ~55 m thick south of Beavertail Bend, and pinches out or thins irregularly. Unit **Mvgssc** is not observed in the BISSA well at depth (S. Reidel, WSU Tri-Cities, written commun., 2020). Unit **Mvgssc** contains at least two or three flows and forms robust cliffs with common basal colonnade, interior entablature, vesicular flow top, and uncommon hyaloclastite horizons. Compared to unit **Mvgssf**, unit **Mvgssc** is more sparsely mapped and inconsistently interfingers with or overlies flows of unit **Mvgssf** (Reidel, 2005, 2015). Unpublished mapping by Bentley and Powell in the early 1980s labels this unit as Toc (Ortley Cohasset?) or Tch (Chinahat/Cohasset?).

Mvgssf Basalt of Spokane Falls (middle Miocene)—Fine-grained basaltic andesite with groundmass crystals ranging in size from 0.1 to 0.4 mm and very rare phenocrysts of plagioclase as large as 1.2 mm; most commonly aphyric; groundmass textures are microcrystalline, range from seriate to equigranular, and pilotaxitic (unoriented). Unit **Mvgssf** has diagnostically higher zirconium and lower chromium values than unit **Mvgssc**, but unit **Mvgssf** can be challenging to distinguish from other subunits of the Sentinel Bluffs Member that have similar geochemistry, particularly the basalt of Museum. Other contents include mafic minerals (20–40%, 0.1–0.4 mm, mostly clinopyroxene), opaque minerals (~40%), and some devitrified glass (0–20%). From map

patterns, unit **Mvgssf** is less than 65 m thick and is more common than unit **Mvgssc**. In the BISSA well, unit **Mvgssf** is ~60 m thick (S. Reidel, WSU Tri-Cities, written commun., 2020). Unit **Mvgssf** contains at least two flows and inconsistently overlies the basalt of Stember Creek (possibly near IVZ), and—as depicted in Reidel (2005, 2015)—may interfinger with the basalt of Stember Creek. Unit **Mvgssf** forms robust cliffs with common basal colonnade, interior entablature, vesicular flow top, and rare hyaloclastite horizons. Unit **Mvgssf** is common at middle elevations. Unpublished mapping by Bentley and Powell in the early 1980s labels this unit as Toj (Ortley Jim?) or Tbt (Bingen unknown designation?).

Mvgssc Basalt of California Creek (middle Miocene)—Fine-grained basaltic andesite; medium gray; strongly weathered; dense; aphyric; exposed only at one locality (geochemistry site G204) from a low outcrop of vesicular top; approximate unit thickness is less than 50 m, may pinch out based on lack of exposure. Lacking more geochemical analyses for support, we interpret only a small lens of unit **Mvgssc** overlying basalt of McCoy Canyon (unit **Mvgsmc**) and underlying basalt of Spokane Falls (unit **Mvgssf**) on the southwest flank of the Boylston Mountains. Given the unit's thickness and single geochemical sample, we cannot rule out that it may be more common than we map due to under-sampling of zones between the basalts of McCoy Canyon and Spokane Falls because of lack of exposure. We report the first instance of this unit identified in the Kittitas Valley.

Mvgsmc Basalt of McCoy Canyon (middle Miocene)—Fine-grained basaltic andesite with groundmass crystals ranging in size from ~0.1 to 0.5 mm and very rare phenocrysts of plagioclase as large as 1.2 mm; most commonly aphyric; groundmass texture is microcrystalline, equigranular, pilotaxitic (unoriented), and uncommonly microvesicular. Some samples we identify as belonging to this unit have similar geochemistry to some

samples we identify as belonging to unit **Mv_{gw}**, but lack the glomerocrysts of the Winter Water Member. The unit includes mafic minerals (5–40%, 0.05–0.5 mm, mostly clinopyroxene) and some devitrified glass (0–10%). From map patterns, unit **Mv_{gsmc}** is ~65–95 m thick, whereas at depth, in the BISSA well, it is at least ~80 m thick (S. Reidel, WSU Tri-Cities, written commun., 2020). Unit **Mv_{gsmc}** contains at least two flows and forms robust cliffs with well-developed entablature with short basal colonnade, and commonly has a vesicular flow top and hyaloclastite horizons near its base. Unit **Mv_{gsmc}** overlies the Winter Water Member and does not contact the Coleman member of the Ellensburg Formation (unit **M_{cec}**). Unit **Mv_{gsmc}** is common at mid to high elevations in Yakima Canyon, or low elevations in the Boylston Mountains, and at the bottom of Park Creek. Unpublished mapping by Bentley and Powell in the early 1980s labels this unit as **Tbb** (Bingen Bumping Hollow?) or **Tmc** (McCoy).

Mv_{gw} Winter Water Member (middle Miocene)—Fine- to medium-grained basaltic andesite; locally aphyric, but may be sparsely to abundantly glomerocrystic to porphyritic, especially outside the map area; medium to dark gray, weathers medium to dark brown; dense. From map patterns, unit **Mv_{gw}** is ~42 m thick in Yakima Canyon, and at depth unit is ~28–98 m thick in the Meridian well (S. Reidel, written commun., WSU Tri-Cities, 2020). Unit **Mv_{gw}** contains at least two flows and forms subdued cliffs—especially compared to overlying unit **Mv_{gsmc}**—with well-developed entablature and common stacks of segmented and tilted basal colonnade, and commonly has a vesicular flow top and hyaloclastite horizons near its base. Unit **Mv_{gw}** underlies the Sentinel Bluffs Member (specifically, the basalt of McCoy Canyon) and overlies the Ortley member. Unit **Mv_{gw}** has a normal magnetic polarity. Contact relationships between Winter Water and Ortley members suggest that unit **Mv_{gw}** may be an intracanyon flow with the underlying Ortley member (unit **Mv_{go}**). Unit **Mv_{gw}** contains numerous closely spaced fractures, joints, and faults(?) in the Boylston Mountains. Note that prior usage of the name “Winter Water flow” referred to a glomerocrystic unit that overlies the aphyric “Umtanum flow” (Reidel and others, 1989),

and they were divided accordingly based on phenocryst abundance. These rocks are now grouped based on their similar geochemical compositions (Reidel and Tolan, 2013), and we mapped mostly the aphyric variety especially near the Yakima canyon area.

Mv_{go} Ortley member (middle Miocene)—Fine- to medium-grained basaltic andesite to andesite with groundmass crystals up to 1 mm in size; most commonly aphyric; groundmass texture is weakly microporphyritic, pilotaxitic (unoriented), and mildly microvesicular (diktytaxitic). Unit **Mv_{go}** and unit **Mv_{gg}** can be difficult to distinguish because they have similar geochemical compositions, however unit **Mv_{go}** is normally magnetized compared to unit **Mv_{gg}**. From map patterns, unit **Mv_{go}** is at least ~46 m thick in Yakima Canyon. At depth, unit **Mv_{go}** is ~230 m thick in the BISSA well and ~215–251 m thick in the Meridian well (S. Reidel, WSU Tri-Cities, written commun., 2020). Unit **Mv_{go}** is widespread at the lower elevations in Yakima Canyon and in deep canyons of the Boylston Mountains. Unit **Mv_{go}** contains two to four flows and commonly forms well-developed vesicular flow tops, entablature, and palagonitic and peperitic hyaloclastite, whereas basal colonnade is rare. In Yakima Canyon, the Ortley member overlies the Grouse Creek member (unit **Mv_{gg}**) and underlies the Winter Water Member (unit **Mv_{gw}**). Unit **Mv_{go}** has a normal magnetic polarity, is part of the N2 MSU, and represents the base of N2 MSU in the map area. Hyaloclastite, pillow breccia, and peperite are also very common in our map area, and the abundance of these three features strongly suggests that unit **Mv_{go}** is invasive, where lavas flow into unconsolidated sediments (invading them). Unpublished mapping by Bentley and Powell in the early 1980s labels this unit as **Tbp** (Bingen unknown designation?) or **Tbw** (Bingen unknown designation?).

Mv_{gg} Grouse Creek member (middle Miocene)—Medium- to fine-grained basaltic andesite with groundmass crystals less than 1.5 mm in size; aphyric; groundmass texture is generally pilotaxitic (unoriented) with groundmass crystal sizes slightly greater than those of unit **Mv_{gs}**. Unit **Mv_{gg}** and unit **Mv_{go}** can be difficult to distinguish because they have similar geochemical compositions, however unit **Mv_{gg}** is reversely magnetized compared to unit **Mv_{go}**. Unit represents the top of R2 MSU in the map area and its base is not observed locally. From map patterns, the unit is greater than 140 m thick and may be thicker based on mapping farther north (Sadowski and others,

2020, 2021), where the base is observed. At depth, unit **Mv_{gg}** is ~90 m thick in the BISSA well and ~46–91 m thick in the Meridian well (S. Reidel, WSU Tri-Cities, written commun., 2020). Unit **Mv_{gg}** contains at least one flow and forms robust cliffs of common fanning entablatures, colonnades, vesicular tops, and lesser autobreccias and some platy entablature. Unit **Mv_{gg}** is well exposed in Yakima Canyon. The unit was mapped as the Howard Creek invasive flow by Rosenmeier (1968), GRB MSU R2 by Tabor and others (1982), the Meeks Table flow by Swanson (1976, 1978), Bentley (1977), and Hammond (2013).

LITHOLOGIES DEPICTED AS OVERLAYS

We depict some units as overlays to highlight underlying bedrock while still showing the distribution of these thin surficial deposits and landforms.

Mass Wasting (overlay mw)

We map mass-wasting overlays in areas where landforms suggest mass movement on unstable slopes, but where evidence for landslide deposits is inconclusive. Overlays mark areas of hummocky or irregular surface morphology that generally lack unambiguous features—head scarps, flanking scarps, and toes—that unit **Qls** may otherwise exhibit. We find that these mass-wasting landforms are more common at higher elevations and may indicate areas of solifluction: gradual downslope mass movements related to freeze-thaw cycles. In places, overlays of loess may overlap what appear to be mass-wasting landforms. In these instances it is unclear if areas where these two overlays are combined are especially prone to mass wasting. In these overlap areas it is also possible that the loess may just be exhibiting an uneven surface that is typical of loess landform development (see overlay **Ql** below), rather than a real mass-wasting feature. The mass-wasting overlay is prolifically mapped in the Boylston Mountains and Yakima Canyon.

Quaternary Loess (overlay Ql)

We map thin accumulations of eolian loess (typically <2 m) with an overlay polygon to avoid obscuring the underlying geologic unit. Loess mantles the majority of bedrock surfaces, and it varies in thickness and form. The absence of a loess overlay does not necessarily indicate the absence of loess. For example, areas of Manastash Ridge are completely blanketed by loess, but we omit an overlay to ensure clarity of the underlying bedrock geology. Loess is light to medium brown; moderately weathered; loose; composed of silt to very fine-grained sand; angular; moderately sorted; structureless and forms ~1–6-m-thick, irregularly spaced mounds (where thin) or hilly exposures (where thick) with varying amounts of post-depositional dissection. Loess is widespread in the map area and especially abundant on the flat to gently sloping north-facing slopes of Manastash Ridge and the Boylston Mountains. Loess blankets older alluvial deposits—especially units **Qaf₃** and **Qaf₄**—and bedrock, but is mostly absent on

younger alluvial surfaces. Though we show folds and faults as certain and unconcealed by this overlay unit, the deposits are not folded and do not appear to be faulted. Loess appears most thickly deposited in low-elevation portions of Badger Pocket and Manastash Ridge, where it accumulates on the leeward and windward sides of the nearby high topography.

Following significant eolian deposition, mound-like landforms composed of loess are produced and sometimes called “Manastash Mounds,” an example of patterned ground that may have resulted from frost action—solifluction with soil creep—under a periglacial climate (Kaatz, 1959; Williams and Masson, 1949). Anastomosing features between mounded loess landforms show ~0.3–6-m-deep incisions that are ~0.6–5 m wide, suggesting that fluvial incision and erosion may also aid generation or modification of these loess landforms. We posit that overland flow from precipitation and snow melt dissects loess to generate at least four stages of loess landform development, from least to most developed: (1) an undissected blanket from eolian processes, (2) partly connected incised landforms with “fluvial” textures, (3) patchy isolated landforms with relict “fluvial” textures, to (4) fully isolated patterned ground with non-uniform mound size and spacing in comparison with Mima mounds, which have more uniform mound size and spacing (Polenz and others, 2017)). Unit **Qls** and overlay **mw** can contain substantial amounts of loess incorporated from nearby loess overlays. Bender and others (2016) report an infrared stimulated luminescence age between 84.2 and 93.3 ka from loess overlying unit **Qg** in Yakima Canyon (age site GD13). Elsewhere, we infer the unit age is approximately Holocene to Pleistocene based on correlation with the Palouse Formation (Busacca, 1989; Sweeney and others, 2017). Overlay **Ql** correlates with the eolian loess of the Palouse Formation.

Miocene Hyaloclastite (overlay hy)

Wherever hyaloclastite is present within or between the basaltic units of the CRBG, we delineate its extent using a map overlay. Hyaloclastite is more commonly found in Wanapum Basalt units **Mv_{wr}** and **Mv_{wfsh}**, and can also crop out near the base of unit **Mv_{gsmc}** and near the tops of units **Mv_{go}** and **Mv_{gsm}**.

Where mapped, hyaloclastite consists of volcanoclastic aggregate of pillow breccia with volcanic glass (tachylyte ±sideromelane) and its alteration product palagonite; light yellowish to orangish brown, strongly weathered; compact, less dense than basalt; composed of sand- to boulder-sized clasts in a very fine-grained matrix; angular to subangular; poorly sorted; some exposures may contain cobble- to boulder-sized fragments of basalt pillows (centimeter- to meter-scale) that are matrix supported (pillow breccia). Where pillows are absent, exposures are convoluted and structureless; pillow fragments have chilled margins and radial interior jointing like entablature. Hyaloclastite thickness varies but is generally less than 30 m thick.

In general, hyaloclastite forms as the result of hot lava interacting with and quenching in water. In a more specific case where lava invades saturated sediments, this generates peperitic hyaloclastite also called peperite. Peperite locally contains entrained sedimentary material among basalt and hyaloclastite material, and is well exposed up southerly draining canyons north of Beavertail Bend and near Vanderbilt Gap.

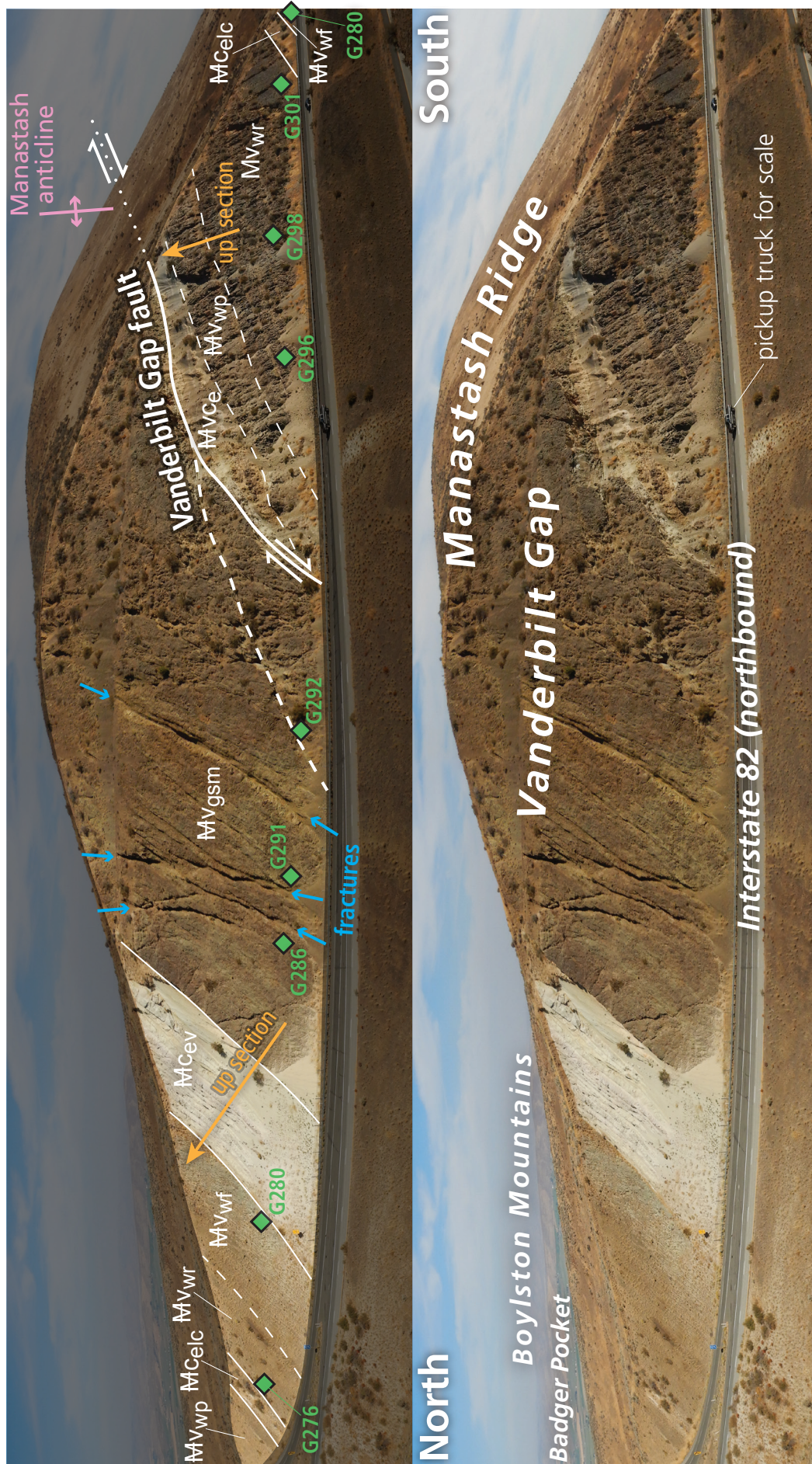


Figure 3. Panoramic photo looking east across interstate 82 at a highway cut in Vanderbilt Gap (Fig. 1). Photo shows the Vanderbilt Gap fault along with a tilted section of Grande Ronde Basalt, Wanapum Basalt, and Ellensburg Formation. Unit labels and descriptions can be found in the Description of Map Units. Thin white lines are depositional contacts and thick lines are faults (both are dashed where inferred). Multiple fractures (blue arrows) are present in the brecciated basalt of Museum (unit Mvgs). Green diamonds are geochemical samples (see Appendix D and Data Supplement).

Near Beavertail Bend, the invasive Ortley basalt (unit **Mvgo**) fully encompasses white, centimeter-scale sedimentary rock fragments with a jigsaw texture (Coleman member?). Near Vanderbilt Gap, the Roza basalt (unit **Mvwr**) invaded Lmuma Creek sediments, which are convoluted among large pillows west of I-82. The spatial association of hyaloclastite, water, and sediment supports the notion that these interactions occurred in lower paleotopographic elevations that preceded or followed the deposition of other lower Ellensburg Formation units. We also infer that Miocene water bodies mark periods of localized eruptive quiescence wherein landscapes had time to establish water bodies that lavas would eventually occupy.

The following mineralogical features are common near in-place and out-of-place hyaloclastite and vesicular tops: fragments of petrified wood, pods, and fragments of common opal (opal-AG, opaque, yellowish green to brownish yellow, ~10–30 cm diameter pods where *in situ*), and thin coatings of hyalite (opal-AN, clear to white, silica globs and crusts <3 cm thick). We posit an association between opaline silica mineraloids and the petrification of Miocene wood (Mustoe, 2023) wherein available free excess silica from the quenching lava replaces cellulose and lignin, and any remaining free excess silica precipitates as opaline silica.

DISCUSSION

Paleoenvironments of the Upper Ellensburg Formation

In the map area, we interpret the following depositional environments for unit **Mvce** based on lithology (intervals A–C on Fig. 2): mudstone and siltstone near the base of the unit suggest lacustrine deposition (A and lower half of B on Fig. 2); abundant, structureless, laminated, or crossbedded sandstones–siltstones we interpret as fluvial floodplain deposits (B on Fig. 2); structureless loess-rich paleosols may mark periods of fluvial quiescence and soil development (B and C on Fig. 2) with pyroclastic material more common up section; and pumiceous, basaltic, or dacitic sandstone lenses or discontinuous beds which may be distal lahar deposits (Fig. 2A,C).

Deposition of unit **Mcge** followed—or slightly overlapped with—deposition of unit **Mvce**. Similar to the interpretations of Smith (1988b), we interpret the following terrestrial depositional environments for unit **Mcge** based on lithology (Fig. 2D,E): structureless fine-grained deposits as paleosols and floodplain deposits (Fig. 2D); thickly bedded deposits of sandstone and siltstone as stream, debris flow, or energetic sheetflow(?) deposits within incised paleochannels; and alternating laminated very fine and medium sandstone as scour-and-fill, floodplain overbank, and low energy sheetflow deposits. Unit **Mcge** likely records competition for accommodation space in Kittitas Valley among the unit's three sediment sources: (1) basaltic colluvium shedding from nearby active folds, (2) debris flow, sheetflow, and floodplain deposits, and (3) waning Cascade-sourced volcanoclastic and pyroclastic deposits. Together, units **Mvce** and **Mcge** exhibit a coarsening upward sequence that suggests an environment with increasing depositional energy over time.

Description of Geologic Structures

Our mapping refines the locations of geologic structures and broadly agrees with the findings of Ladinsky and Kelsey (2012), Kelsey and others (2017), and Staisch and others (2018a).

MANASTASH RIDGE

The Manastash Ridge range front has a broad, gently sloping piedmont with abundant Miocene to Pliocene(?) gravels and Quaternary fans. High on this piedmont, we map a major south-east-striking range front thrust fault that we name the Manastash thrust—also known as the “frontal fault” of Kelsey and others (2017) and the Manastash Creek-Hanson Creek Fault of Bentley (1977). We map two major asymmetric plunging anticlines near Manastash Ridge. These two major west-northwest-trending anticlines are the Manastash and Thrall anticlines—both named by Bentley (1977)—and are >2 km or <1 km from the main thrust, respectively. Based on their locations in the hanging wall of the Manastash thrust, we infer that these anticlines are fault-related folds which may be associated with a possible ramp-flat geometry under Manastash Ridge. This inference broadly agrees with the findings of Ladinsky and Kelsey (2012), Kelsey and others (2017), and Staisch and others (2018a). We agree with these studies insofar as the folds are fault-related, and that there are likely low-angle thrust geometries locally, but we interpret a slightly different structural geometry for these faults and folds based on our detailed mapping and geophysical modeling (see *Geophysical Anomalies near the Boylston Mountains and Manastash Ridge*).

Based on uplift rates from recently deformed Quaternary alluvial fans, Ladinsky and Kelsey (2012) conclude that the Manastash anticline is an active fold related to active frontal faulting. We extend this inferred activity to the Thrall anticline because it is associated with the same thrust fault. Based on their respective fold geometries, we tentatively interpret the Manastash anticline as a fault bend fold and the Thrall anticline as a fault propagation fold.

We also map a questionable west–northwest-striking reverse fault north of the monoclinical hinge of the Manastash anticline in the southwest map area. Possible evidence for this fault includes a subparallel linear valley containing abundant breccia. This questionable reverse fault may be a right step of the “backthrust” of Kelsey and others (2017). However, folding of the nearby faulted and tightly folded Thrall syncline could also explain these observations.

The best-exposed fault in the map area is exposed at a roadcut on the east side of Vanderbilt Gap (Fig. 3). We name it the Vanderbilt Gap fault. It is a west–northwest-striking, northeast-dipping fault that cuts through Manastash Ridge and is probably a backthrust of the Manastash thrust. At Vanderbilt Gap, the fault is shallowly dipping (<30 degrees) near the ridgeline and moderately dipping (51 degrees) lower near the road level (Fig. 3).

Based on how the trace of the fault interacts with topography, we infer the backthrust also changes dip along strike. Northwest of geochemistry site G251, the fault is steeply dipping (reverse) while southeast of G251 it is shallowly dipping (thrust). We infer from map patterns that the Manastash anticline formed before being faulted by the Vanderbilt Gap fault.

BOYLSTON MOUNTAINS

Along the Boylston Mountains, we map a long (>16 km) north-west-striking, steeply northeast-dipping reverse fault that we name the Boylston fault, which offsets middle Miocene and potentially younger rocks. Several short discontinuous faults in the hanging wall show oblique slickenlines that suggest these faults—and possibly the Boylston fault—have an oblique sense of slip and may be responding in a transpressional sense. We also map a major ridgecrest-forming, northwest-plunging anticline in its hanging wall called the Boylston anticline (Bentley, 1977). We interpret this fold to be fault related because of its close spatial relationship to the Boylston fault. We map another major ridgecrest-forming, east-plunging anticline in the southeastern map area, which may be related to the Saddle Mountains anticline and Saddle Mountains thrust based on mapping by Bentley (1977) and unpublished mapping (R. Bentley and J. Powell, Central Washington University, unpub. mapping, 1980–1989). Both structures terminate in our map area. The two prominent ridgecrest-forming anticlines are separated by a cluster of faults near a bend in the crest of the Boylston Mountains (see *Northerly Striking Faults*). This separation and change in fold axis trend are conspicuously similar to northerly adjacent mapping (Sadowski and others, 2022), where the northwest-trending Whiskey Ridge anticline and the west-trending Whiskey Dick anticline are separated by a fault near Park Creek.

We map numerous escarpments in the footwall of the Boylston fault, some of which may be fault-related whereas others may be related to agricultural activities (for example, buried irrigation lines). Additional scarps could be mapped but are obscured by thin colluvial or loess material on units Qaf4 or Mv_wfsH especially near the mouth of Wippel Creek.

NORTHERLY STRIKING FAULTS (NSFs)

From lidar and Google Earth imagery, we map numerous closely spaced, steeply dipping cross faults with north through northeast strikes in the Boylston Mountains. We collectively refer to these structures as ‘northerly striking faults’ (NSFs), similar to Sadowski and others (2021, 2022). NSFs form conspicuous scarps through Miocene bedrock. We infer most NSFs to have meter-scale displacements because most NSFs do not visibly offset contacts or fold axes on the map, particularly for shorter fault strands. However, longer NSFs show greater amounts of offset with oblique slip of tens to hundreds of meters. The most prominent NSF is a northeast-striking dextral reverse fault named the Johnson Canyon fault by Barnett and others (2013), which produced the “Boyleston [*sic*] Ridge scarp” of Kelsey and others (2017). We are unclear of the relative ages between the Johnson Canyon and Boylston faults because we lack evidence of the Johnson Canyon fault cutting the Boylston fault. We show it only in the hanging wall like other NSFs.

Most NSFs cluster near a bend in the ridgeline of the Boylston Mountains and roughly demarcate a distinct change in structural style, where west of this fault cluster, folds trend northwest, and east of this fault cluster, folds trend west. We speculate that NSFs clustered here may be associated with a structural boundary—possibly as tear faults—and (or) formed in response to proximal folding. The Meridian well is located

in the middle of numerous closely spaced NSFs, and this may impact subsurface observations of unit thicknesses.

There are fewer NSFs near Manastash Ridge compared to the Boylston Mountains. We map one NSF based on a structural discordance over a short distance near Vanderbilt Gap and infer an eastside-up sense of slip based on map patterns and some possible dextral motion based on the north–south compressional regime. It is possible, but not necessary, that this NSF truncates the Manastash thrust.

Discussion of Geophysical Anomalies

We present a combined gravity and aeromagnetic geophysical anomaly map (Figure M1A) and two possible geophysical models (Figs. M1B, M1C) that support our interpretations in the geologic cross sections. The geophysical models are particularly sensitive to the depth and geometry of the N2–R2 magnetostratigraphic boundary, thickness changes of normal and reverse rock packages (N2, R2, Mv_{wp} and Mv_{wr}), the thickness of Quaternary and upper Ellensburg units above the CRBG (collectively referred to as Quaternary–Miocene sedimentary material, which is also a proxy for depth to CRBG), and depth-to-basement contact with Eocene sedimentary rocks. Geophysical data that we present cannot confirm exact thicknesses of CRBG units, but can support changes in elevation or thickness within certain packages. Southeast of the map area, a nearby resistivity profile by Wilt and others (1989) shows a varying thickness of total CRBG rocks that independently agrees with the total CRBG thickness we show in our models. Individual flow thicknesses within these larger packages are better constrained by the mapping and well data presented here.

GEOPHYSICAL ANOMALIES NEAR THE BOYLSTON MOUNTAINS AND MANASTASH RIDGE

Linear aeromagnetic and gravity anomalies show evidence for frontal fault zones along the southern margin of the Boylston Mountains and the northern margin of Manastash Ridge (Boylston fault zone and Manastash fault zone, ‘BFZ’ and ‘MFZ’ respectively, Fig. M1A). Max spots delineate two moderate magnitude (~7 mGal) linear gravity gradients along the mountain fronts that are best fit by models featuring range-bounding reverse faults and lower-angle splays. A very low angle thrust best fits the data for the MFZ, and a moderately-dipping (45–55 degrees) fault best fits data for the BFZ. Along the BFZ, simultaneously fitting the gravity (fault tip lows, ‘FTL’ on Figs. M1B and M1C), flanking aeromagnetic data (Fig. M1A), and surface geology requires models that offset the top of the CRBG and younger units, along with thicker accumulations of Quaternary–Miocene sedimentary packages in the footwall (growth strata). This suggests late Miocene and younger fault activity.

An especially strong aeromagnetic low flanks the BFZ to the northeast (250–750 nT; Boylston Aeromagnetic Low, ‘BAL’ on Figs. M1A–C), supporting the presence of a broad, asymmetric northwest-plunging anticline. The best-fit model and surface geology also suggest the southwest limb is faulted by the BFZ. Thickened reverse polarity Wanapum units in the footwall of the low angle splay faults provide a best fit of a broad aeromagnetic low southwest of the BFZ (~100 nT; Wanapum

aeromagnetic low, 'WAL' on Fig. M1C), potentially indicating syn-depositional deformation.

Two small faults northeast of the BFZ (Boylston Anticline faults, 'BAF1' and 'BAF2' on Fig. M1B) help fit small amplitude gravity inflections that flank a large aeromagnetic high (~270 nT; northeast aeromagnetic high, 'NEAH' on Fig. M1B). These faults may dip less steeply than we depict; the offsets are so small that we lose resolution with depth. Thickening and thinning of R1, N1, and R2 magnetostratigraphic units (MSU) at depth across these two faults are required to fit the aeromagnetic anomaly NEAH, but the exact geometry is not well-constrained, therefore we show a model with minimal thickness change.

In contrast to the aeromagnetic low along the BFZ, the MFZ has a linear aeromagnetic high along the crest of the Manastash Ridge (Manastash aeromagnetic high, 'MAH' on Fig. M1A). There is also a strong aeromagnetic low (Manastash aeromagnetic low, 'MAL' on Fig. M1A) over the Yakima River, where we map unit **Mv_{gg}**, which has reversed magnetic remanence. Both anomalies have high amplitudes (+400 nT and -760 nT, respectively) and are bounded by steep gradients, indicating structural sources in the upper 1,000 m of the crust. Doubling the thicknesses of N2 MSU and R2 MSU in adjacent locations at this depth (under MAH and MAL, respectively, in Fig. M1C) is required to fit both aeromagnetic anomalies. This finding strongly influenced our positioning and geometry of the Manastash thrust in cross section A–A'. A single low-angle thrust fault with ramp-flat geometries can generate these two thickness duplications, and helps explain breccias in unit **Mv_{gg}** where this fault would come close to the surface in Yakima Canyon.

When compared to the geophysical modeling of Staisch and others (2018a) and the structural models of Kelsey and others (2017), our ramp-flat interpretation differs somewhat in the exact location and geometry of faults, and therefore the amount of slip on those faults. We attribute these differences to our detailed geologic mapping, newly collected gravity measurements, and well-constrained rock properties. Our models also suggest folding started at the Manastash front before the thrust cut through the folded stratigraphy of the Thrall anticline, which agrees with Kelsey and others (2017). Modeling by Staisch and others (2018a, their figure 10c) shows a south-dipping fault near Manastash Ridge continuing southward to great depth, which offsets Miocene and pre-Miocene strata. Although not shown in our modeling (lower left of Figure M1C), we recognize that such a fault or a blind fault is possible at this location, but is not required by our modeling.

Hyaloclastite and (or) fault breccia may explain low-amplitude fluctuations in gravity anomalies (~2 mGal) near BFZ and in the hanging wall of MFZ. Anastomosing gravity max spots collocated near discontinuous aeromagnetic lows may suggest *en echelon* faults along mountain fronts. Alternatively, these could be related to minor folding or stratigraphic thickness changes. However, a local change in trend of max spots and a gravity high near Vanderbilt Gap (Manastash High, 'MH' on Fig. M1A) supports the existence of a north–south striking fault mapped at the surface.

GEOPHYSICAL ANOMALIES IN KITTITAS VALLEY AND BADGER POCKET

We account for the gravity low (Kittitas Valley low, 'KVL' on Fig. M1A) between the BFZ and MFZ by increasing the thickness of the Quaternary–Miocene sedimentary package and increasing depth to basement in the center of the Kittitas Valley. Abundant well data intersecting the top of the CRBG near the fault zones constrain the thickness of the Quaternary–Miocene sedimentary package, which in turn constrains deeper parts of the model. In most places, a simple fold or gentle ramp on the CRBG top can account for small amplitude, short wavelength gravity anomalies across the Kittitas Valley (Kittitas Valley gradient, 'KVG' on Fig. M1A). We do model one vertical fault with moderate vertical offset to fit a short-wavelength, ~0.5 mGal drop in gravity (Kittitas Valley fault, 'KVF' on Fig. M1B); other fault dips are possible given the small amplitude of the gravity anomaly.

RECOMMENDATIONS FOR FUTURE RESEARCH

- Investigate stability of areas with young alluvial fans, landslide deposits, tilted Miocene sedimentary rocks, and mass-wasting landforms, especially in proximity to major transportation infrastructure (for example, near I-82/US 97 or SR 821).
- Perform paleoseismic investigations to assess faults and scarps of unknown origin, especially those in alluvial fan units on Manastash Ridge and the Boylston Mountains, to determine timing and recurrence of faulting.
- Investigate deep well logs in the footwall of the Manastash frontal fault to assess the geometry of short wavelength folding of Wanapum Basalt and any possible relationship to range front faulting.
- Characterize the provenance and volcanoclastic sedimentology of the upper Ellensburg Formation. Similar to work of Humphrey (1996), research could include whole-rock geochemistry and tephrochronology of accretionary lapilli tuff marker beds below age site GD09, investigating the volcanic source of dacite clasts, and further analyses of detrital zircon age spectra.
- Characterize the provenance of units **M_{cev}** and **M_{celc}** with additional U–Pb age sites near Vanderbilt Gap and compare their respective age spectra near Yakima Canyon to assess any temporal-spatial changes in provenance.
- Collect and interpret a drone-based photo panorama of Potato Hill to understand the sedimentology of upper Ellensburg Formation unit **M_{cge}**.
- Geophysical modeling of a northwest–southeast profile that crosses a ~2.7-km-wide, northeast-trending moderate magnetic high in Badger Pocket subparallel to Cross Section A–A'. We wonder if this anomaly represents a structure, but lack an orthogonal transect to interpret this anomaly further.

ACKNOWLEDGMENTS

We thank, from CWU: Nick Zentner, Walter Szeliga, Lisa Ely, Chris Mattinson, Hannah Shamloo, and many faculty of the Geology Department for many meaningful conversations and field trips. From WGS, we thank: Alex Steely, Michael Polenz, Trevor Contreras, and Becca Goughnour for initial reviews of the map, cross section, and report text. We thank Todd Lau and Anita Bauer for collecting the new gravity data. We also thank Ashley Cabibbo and Ian Hubert for GIS data stewardship and quality control. From Villanova University, we thank Isabel Hong for identifying our diatoms (formerly of CWU). From USGS, we thank Steve Angster, Ralph Haugerud, and Lydia Staisch for help synthesizing past and on-going regional work. Of emeritus investigators, we thank Terry Tolan, Stephen Reidel, Gary A. Smith, and Ray Wells for clarifying structural and stratigraphic questions. Of WSU, thanks to Ashley Steiner, John Wolff, and the whole staff at the WSU Peter Hooper GeoAnalytical lab in Pullman, WA for analyzing geochemistry samples and classifying CRBG rocks using their Machine Learning (ML) model. Also from WSU, thanks to Jeff Vervoort and Vic Valencia (ZirChron LLC) for analyzing our detrital zircon samples in the Radiogenic Isotope and Geochronology Laboratory (RIGL). We thank Jim Landon for his classification of our petrified wood sample. We also thank Thomas Lapen and Shawn Fields of University of Houston for sharing their new age data from Craigs Hill. We also thank Skye Cooley for meaningful discussions about Columbia basin stratigraphy and Quaternary escarpments. Of private citizens, we thank John Eaton and the Eaton Family, Craig Clerf, Ed Ricard, Tom Nesbitt, Martha Pilcher, and Jim Broadlick, and countless other private landowners, ranchers, farmers, and businesses for general assistance or land access. We also thank the Yakima Training Center (Department of Defense), Zirkle Fruit, Ellensburg Cement, Kittitas Reclamation District (KRD), and Cascade Irrigation District for access through or around their properties.

AUTHOR CONTRIBUTIONS

Geologic mapping was performed by A. Sadowski and L. Wetherell together in most of the map area. L. Wetherell performed solo fieldwork in the mid to low elevations of Manastash Ridge, near the mouth of Wippel Creek and north of the meander of Yakima River. Geophysical data were interpreted and modeled by M. Anderson with contributions from T. Lau. Writing of the pamphlet was completed by A. Sadowski, M. Anderson, and L. Wetherell. A. Sadowski wrote most of the text with M. Anderson providing contributions in *Methods*, Appendices A, B, C, and D, and *Discussion of Geophysical Anomalies*. J. Powell conceptualized early drafts of the cross sections, provided guidance on stratigraphic and structural framework, and reviewed early drafts of map, cross sections, and text. GeMS data schema and Data Supplement were populated by A. Sadowski. Map GIS linework, geologic analysis, and geologic cross section construction were performed by A. Sadowski and L. Wetherell. Figure 2, Cross Section B–B', and map GIS linework in the vicinity were completed by L. Wetherell.

REFERENCES

- Allmendinger, R. W.; Cardozo, Nestor; Fisher, D. M., 2012, Structural geology algorithms: Vectors and tensors: Cambridge University Press, 289 p.
- Barnes, D. F.; Oliver, H. W.; Robbins, S. L., 1969, Standardization of gravimeter calibrations in the geological survey: *Eos, Transactions American Geophysical Union*, v. 50, no. 10, p. 626–627. [https://doi.org/10.1029/EO050i010p00526]
- Barnett, E. A.; Sherrod, B. L.; Norris, Robert; Gibbons, Douglas, 2013, Paleoseismology of a newly discovered scarp in the Yakima fold-and-thrust belt, Kittitas County, Washington: U.S. Geological Survey Scientific Investigations Map 3212. [http://pubs.usgs.gov/sim/3212]
- Barry, T. L.; Kelley, S. P.; Reidel, S. P.; Camp, V. E.; Self, S.; Jarboe, N. A.; Duncan, R. A.; Renne, P. R., 2013, Eruption chronology of the Columbia River Basalt Group. *In* Reidel, S. P.; Camp, V. E.; Ross, M. E.; Wolff, J. A.; Martin, B. S.; Tolan, T. L.; Wells, R. E., editors, The Columbia River flood basalt province: Geological Society of America Special Paper 497, p. 45–66.
- Bender, A. M.; Amos, C. B.; Bierman, Paul; Rood, D. H.; Staisch, Lydia; Kelsey, Harvey; Sherrod, Brian, 2016, Differential uplift and incision of the Yakima River terraces, central Washington State: *Journal of Geophysical Research Solid Earth*, v. 121, no. 1, p. 365–384. [https://doi.org/10.1002/2015JB012303]
- Bentley, R. D., 1977, Stratigraphy of the Yakima basalts and structural evolution of the Yakima ridges in the western Columbia Plateau. *In* Brown, E. H.; Ellis, R. C., editors, *Geology excursions in the Pacific Northwest*: Geological Society of America, p. 339–390.
- Bingham, J. W.; Grolier, M. J., 1966, The Yakima Basalt and Ellensburg Formation of south-central Washington: U.S. Geological Survey Bulletin 1224-G, 15 p. [http://pubs.er.usgs.gov/publication/b1224G]
- Black, L. P.; Kamo, S. L.; Allen, C. M.; Davis, D. W.; Aleinikoff, J. N.; Valley, J. W.; Mundil, Roland; Campbell, I. H.; Korsch, R. J.; Williams, I. S.; Foudoulis, Chris, 2004, Improved $^{206}\text{Pb}/^{238}\text{U}$ microprobe geochronology by the monitoring of a trace-element-related matrix effect; SHRIMP, ID-TIMS, ELA-ICP-MS and oxygen isotope documentation for a series of zircon standards: *Chemical Geology*, v. 205, no. 1–2, p. 115–140. [https://doi.org/10.1016/j.chemgeo.2004.01.003]
- Blakely, R. J.; Sherrod, B. L.; Weaver, C. S.; Wells, R. E.; Rohay, A. C.; Barnett, E. A.; Knepprath, N. E., 2011, Connecting the Yakima fold and thrust belt to active faults in the Puget Lowland, Washington: *Journal of Geophysical Research Solid Earth*, v. 116, no. B7, 33 p. [https://doi.org/10.1029/2010JB008091]
- Blakely, R. J.; Sherrod, B. L.; Weaver, C. S.; Wells, R. E.; Rohay, A. C., 2014, The Wallula fault and tectonic framework of south-central Washington State, as interpreted from magnetic and gravity anomalies: *Tectonophysics*, v. 624–625, p. 32–45. [https://doi.org/10.1016/j.tecto.2013.11.006]
- Blakely, R. J.; Sherrod, B. L.; Weaver, C. S., 2020a, High-resolution aeromagnetic survey of the Wenatchee area, Washington: U.S. Geological Survey data release. [https://doi.org/10.5066/P9EURKIG]
- Blakely, R. J.; Sherrod, B. L.; Weaver, C. S., 2020b, High-resolution aeromagnetic survey of the Cle Elum area, Washington: U.S. Geological Survey data release. [https://doi.org/10.5066/P9C9MADW]
- Brocher, T. M.; Wells, R. E.; Lamb, A. P.; Weaver, C. S., 2017, Evidence for distributed clockwise rotation of the crust in the northwestern United States from fault geometries and focal mechanisms: *Tectonics*, v. 36, no. 5, p. 787–818. [https://doi.org/10.1002/2016TC004223]
- Busacca, A. J., 1989, Long Quaternary record in eastern Washington, U.S.A., interpreted from multiple buried paleosols in loess: *Geoderma*, v. 45, no. 2, p. 105–122. [https://doi.org/10.1016/0016-7061(89)90045-1]

- Cardozo, Nestor; Allmendinger, R. W., 2013, Spherical projections with OSXStereonet: Computers & Geosciences, v. 51, p. 193–205. [https://doi.org/10.1016/j.cageo.2012.07.021]
- Chang, Zhaoshan; Vervoort, J. D.; McClelland, W. C.; Knaack, Charles, 2006, U-Pb dating of zircon by LA-ICP-MS: Geochemistry, Geophysics, Geosystems, v. 7, no. 5, 14 p. [https://doi.org/10.1029/2005GC001100]
- Czajkowski, J. L.; Bowman, J. D.; Schuster, J. E.; Wheeler, C. M., 2012, Oil and gas wells in Washington State: Washington Division of Geology and Earth Resources Open File Report 2012-02 (rev. 2015), 4 p., 1 Microsoft Excel file with 4 p. text. [http://www.dnr.wa.gov/Publications/ger_ofr2012-02_oil_and_gas_wells.zip]
- Donaghy, E. E.; Umhoefer, P. J.; Eddy, M. P.; Miller, R. B.; LaCasse, Taylor, 2021, Stratigraphy, age, and provenance of the Eocene Chumstick basin, Washington Cascades; Implications for paleogeography, regional tectonics, and development of strike-slip basins: Geological Society of America Bulletin, v. 133, no. 11–12, p. 2418–2438. [https://doi.org/10.1130/B35738.1]
- Ebinghaus, Alena; Jolley, D. W.; Hartley, A. J., 2015, Extrinsic forcing of plant ecosystems in a large igneous province: The Columbia River flood basalt province, Washington State, USA: Geology, v. 43, no. 12, p. 1107–1110. [https://doi.org/10.1130/G37276.1]
- Eddy, M. P.; Bowring, S. A.; Umhoefer, P. J.; Miller, R. B.; McLean, N. M.; Donaghy, E. E., 2016, High-resolution temporal and stratigraphic record of Siletzia's accretion and triple junction migration from nonmarine sedimentary basins in central and western Washington: Geological Society of America Bulletin, v. 128, no. 3–4, p. 425–441. [https://doi.org/10.1130/B31335.1]
- Eddy, M. P.; Umhoefer, P. J.; Miller, R. B.; Donaghy, E. E.; Gundersen, Melissa; Senes, F. I., 2017, Sedimentary, volcanic, and structural processes during triple-junction migration: Insights from the Paleogene record in central Washington. In Haugerud, R. A.; Kelsey, H. M., editors, From the Puget Lowland to east of the Cascade Range: Geologic excursions in the Pacific Northwest: Geological Society of America Field Guide 49, p. 143–174. [https://doi.org/10.1130/2017.0049(07)]
- Fields, S. A., 2023, Geochemical investigations into a Miocene/Pliocene tephra which may constrain the timing of Cervidae in North America: University of Houston Senior Honors Thesis, 52 p.
- Hammond, P. E., 2013, Distribution, stratigraphy, and structure of the Grande Ronde Basalt in the upper Naches River basin, Yakima and Kittitas Counties, Washington. In Reidel, S. P.; Camp, V. E.; Ross, M. E.; Wolff, J. A.; Martin, B. S.; Tolan, T. L.; Wells, R. E., editors, The Columbia River flood basalt province: Geological Society of America Special Paper 497, p. 363–400. [https://doi.org/10.1130/2013.2497(15)]
- Heiskanen, W. A.; Vening-Meinesz, F. A., 1958, The Earth and its gravity field: McGraw-Hill Book Company, Inc., 470 p.
- Hoyt, C. L., 1961, The Hammond sill—An intrusion in the Yakima Basalt near Wenatchee, Washington: Northwest Science, v. 35, no. 2, p. 58–64.
- Humphrey, C. C., 1996, Correlation of the upper Ellensburg Formation with the Old Scab Mountain eruptive center, east-central Cascade Range, Washington: Portland State University Master of Science thesis, 201 p. [https://doi.org/10.15760/etd.7160]
- International Union of Geodesy and Geophysics, 1971, Geodetic reference system 1967: International Association of Geodesy Special Publication no. 3, 116 p.
- Johnson, S. Y., 1985, Eocene strike-slip faulting and nonmarine basin formation in Washington. In Biddle, K. T.; Christie-Blick, Nicholas, editors, Strike-slip deformation, basin formation, and sedimentation: Society of Economic Paleontologists and Mineralogists Society for Sedimentary Geology Special Publication 37, p. 283–302. [https://doi.org/10.2110/pec.85.37.0265]
- Kaatz, M. R., 1959, Patterned ground in central Washington; A preliminary report: Northwest Science, v. 33, no. 4, p. 145–156.
- Kasbohm, Jennifer; Schoene, Blair, 2018, Rapid eruption of the Columbia River flood basalt and correlation with the mid-Miocene climate optimum: Science Advances, v. 4, no. 9, 8 p. [https://doi.org/10.1126/sciadv.aat8223]
- Kasbohm, Jennifer; Schoene, Blair; Mark, D. F.; Murray, Joshua; Reidel, Stephen; Szymanowski, Dawid; Barfod, Dan; Barry, Tiffany, 2023, Eruption history of the Columbia River Basalt Group constrained by high-precision U-Pb and $^{40}\text{Ar}/^{39}\text{Ar}$ geochronology: Earth and Planetary Science Letters, v. 617, 118269. [https://doi.org/10.1016/j.epsl.2023.118269]
- Kelsey, H. M.; Ladinsky, T. C.; Staisch, Lydia; Sherrod, B. L.; Blakely, R. J.; Pratt, T. L.; Stephenson, W. J.; Odum, J. K.; Wan, Elmira, 2017, The story of a Yakima fold and how it informs late Neogene and Quaternary backarc deformation in the Cascadia subduction zone, Manastash anticline, Washington, USA: Tectonics, v. 36, no. 10, p. 2085–2107. [https://doi.org/10.1002/2017TC004558]
- Ladinsky, T. C., 2012, Late quaternary evolution of the Manastash Anticline and Manastash range front, Yakima Fold Belt, Washington—influence of tectonics and climate: California State Polytechnic University, Humboldt, Master of Science thesis, 85 p. [https://scholarworks.calstate.edu/downloads/h128nh254]
- Ladinsky, T. C.; Kelsey, H. M., 2012, Late Quaternary landscape evolution and deformation in the forelimb region of the Manastash anticline, Yakima fold belt, Washington: U.S. Geological Survey National Earthquake Hazards Reduction Program Final Technical Report, 39 p. [https://earthquake.usgs.gov/cfusion/external_grants/reports/G10AC00686.pdf]
- Lanphere, M. A.; Baadsgaard, Halfdan, 2001, Precise K–Ar, $^{40}\text{Ar}/^{39}\text{Ar}$, Rb–Sr and U/Pb mineral ages from the 27.5 Ma Fish Canyon Tuff reference standard: Chemical Geology, v. 175, no. 3–4, p. 653–671. [https://doi.org/10.1016/S0009-2541(00)00291-6]
- Ludwig, K. R., 2012, Isoplot 4.16: A geochronological toolkit for Microsoft Excel: Berkeley Geochronological Center Special Publication no. 5, 75 p.
- Mackin, J. H., 1961, A stratigraphic section in the Yakima Basalt and the Ellensburg Formation in south-central Washington: Washington Division of Mines and Geology Report of Investigations 19, 45 p. [http://www.dnr.wa.gov/publications/ger_r19_strat_yakima_basalt_ellensburg_form.pdf]
- Martin, B. S., 1989, The Roza Member, Columbia River Basalt Group; Chemical stratigraphy and flow distribution. In Reidel, S. P.; Hooper, P. R., editors, Volcanism and tectonism in the Columbia River flood-basalt province: Geological Society of America Special Paper 239, p. 85–104. [https://doi.org/10.1130/SPE239-p85]
- Martin, B. S.; Tolan, T. L.; Reidel, S. P., 2013, Revisions to the stratigraphy and distribution of the Frenchman Springs Member, Wanapum Basalt. In Reidel, S. P.; Camp, V. E.; Ross, M. E.; Wolff, J. A.; Martin, B. S.; Tolan, T. L.; Wells, R. E., editors, The Columbia River flood basalt province: Geological Society of America Special Paper 497, p. 155–180. [https://doi.org/10.1130/2013.2497(06)]
- McCaffrey, Robert; King, R. W.; Payne, S. J.; Lancaster, Matthew, 2013, Active tectonics of northwestern U. S. inferred from GPS-derived surface velocities: Journal of Geophysical Research Solid Earth, v. 118, no. 2, p. 709–723. [https://doi.org/10.1029/2012JB009473]
- McDonald, E. V.; Busacca, A. J., 1992, Late Quaternary stratigraphy of loess in the Channeled Scabland and Palouse regions of Washington State: Quaternary Research, v. 38, no. 2, p. 141–156. [https://doi.org/10.1016/0033-5894(92)90052-K]
- McMillan, Kent; Long, P. E.; Cross, R. W., 1989, Vesiculation in Columbia River Basalts. In Reidel, S. P.; Hooper, P. R., editors, Volcanism and tectonism in the Columbia River flood-basalt province: Geological Society of America Special Paper 239, p. 157–167. [https://doi.org/10.1130/SPE239-p157]

- Morelli, Carlo; Gantar, C.; Honkasalo, Tauno; McConnel, R. K.; Tanner, J. G.; Szabo, Bela; Uotila, Urho; Whalen, C. T., 1974, The international gravity standardization net 1971 (IGSN71): International Association of Geodesy Special Publication No. 4, 194 p.
- Mustoe, G. E., 2023, Silicification of wood: An overview: *Minerals*, v. 12, no. 2, 47 p. [https://doi.org/10.3390/min13020206]
- Nilsen, T. H., 1976, Washington gravity base station network: Washington Division of Geology and Earth Resources Information Circular 59, 83 p.
- Paces, J. B.; Miller J. D., Jr., 1993, Precise U-Pb ages of Duluth Complex and related mafic intrusions, northeastern Minnesota: Geochronological insights to physical, petrogenetic, paleomagnetic, and tectonomagmatic processes associated with the 1.1 Ga Midcontinent Rift System: *Journal of Geophysical Research*, v. 98, no. B8, p. 13,997–14,013. [https://doi.org/10.1029/93JB01159]
- Paton, Chad; Hellstrom, John; Paul, Bence; Woodhead, Jon; Hergt, Janet, 2011, Iolite: Freeware for the visualization and processing of mass spectrometric data: *Journal of Analytical Atomic Spectrometry*, v. 26, p. 2508–2518. [https://doi.org/10.1039/C1JA10172B]
- Phillips, J. D.; Hansen, R. O.; Blakely, R. J., 2007, The use of curvature in potential-field interpretation: *Exploration Geophysics*, v. 38, p. 111–119. [https://doi.org/10.1071/EG07014]
- Plouff, D., 2000, Field estimates of gravity terrain corrections and Y2K-compatible method to convert from gravity readings with multiple base stations to tide- and long-term drift-corrected observations: U.S. Geological Survey Open-File Report 00-140, 37 p. [https://pubs.usgs.gov/of/2000/0140/]
- Porter, S. C., 1976, Pleistocene glaciation in the southern part of the north Cascade Range, Washington: *Geological Society of America Bulletin*, v. 87, no. 1, p. 61–75. [https://doi.org/10.1130/0016-7606(1976)87<61:PGITSP>2.0.CO;2]
- Prakash, Uttam; Barghoorn, E. S., 1961a, Miocene fossil woods from the Columbia basalts of central Washington: *Arnold Arboretum Journal*, v. 42, no. 2, p. 165–203.
- Prakash, Uttam; Barghoorn, E. S., 1961b, Miocene fossil woods from the Columbia basalts of central Washington, II: *Arnold Arboretum Journal*, v. 42, no. 3, p. 347–362.
- Reidel, S. P.; Scott, G. R.; Bazard, D. R.; Cross, R. W.; Dick, Brian, 1984, Post-12 million year clockwise rotation in the central Columbia Plateau, Washington: *Tectonics*, v. 3, no. 2, p. 251–273. [https://doi.org/10.1029/TC003i002p00251]
- Reidel, S. P.; Fecht, K. R.; Hagood, M. C.; Tolan, T. L., 1989, The geologic evolution of the central Columbia Plateau. *In* Reidel, S. P.; Hooper, P. R., editors, *Volcanism and tectonism in the Columbia River flood-basalt province*: Geological Society of America Special Paper 239, p. 247–264. [https://doi.org/10.1130/SPE239-p247]
- Reidel, S. P., 2005, A lava flow without a source: The Cohasset flow and its compositional components, Sentinel Bluffs Member, Columbia River Basalt Group: *Journal of Geology*, v. 113, no. 1, p. 1–21. [https://doi.org/10.1086/425966]
- Reidel, S. P.; Tolan, T. L., 2013, The Grande Ronde Basalt, Columbia River Basalt Group. *In* Reidel, S. P.; Camp, V. E.; Ross, M. E.; Wolff, J. A.; Martin, B. S.; Tolan, T. L.; Wells, R. E., editors, *The Columbia River flood basalt province*: Geological Society of America Special Paper 497, p. 117–154. [https://doi.org/10.1130/2013.2497(05)]
- Reidel, S. P.; Camp, V. E.; Tolan, T. L.; Martin, B. S., 2013a, The Columbia River flood basalt province: Stratigraphy, areal extent, volume, and physical volcanology. *In* Reidel, S. P.; Camp, V. E.; Ross, M. E.; Wolff, J. A.; Martin, B. S.; Tolan, T. L.; Wells, R. E., editors, *The Columbia River flood basalt province*: Geological Society of America Special Paper 497, p. 1–44. [https://doi.org/10.1130/2013.2497(01)]
- Reidel, S. P.; Camp, V. E.; Tolan, T. L.; Kauffman, J. D.; Garwood, D. L., 2013b, Tectonic evolution of the Columbia River flood basalt province. *In* Reidel, S. P.; Camp, V. E.; Ross, M. E.; Wolff, J. A.; Martin, B. S.; Tolan, T. L.; Wells, R. E., editors, *The Columbia River flood basalt province*: Geological Society of America Special Paper 497, p. 293–324. [https://doi.org/10.1130/2013.2497(12)]
- Reidel, S. P.; Camp, V. E.; Ross, M. E.; Wolff, J. A.; Martin, B. S.; Tolan, T. L.; Wells, R. E., editors, 2013c, *The Columbia River flood basalt province*: Geological Society of America Special Paper 497, 440 p. [https://doi.org/10.1130/SPE497]
- Reidel, S. P., 2015, Igneous rock associations 15. The Columbia River Basalt Group: A flood basalt province in the Pacific Northwest, USA: *Geoscience Canada*, v. 42, no. 1, p. 151–168.
- Rosenmeier, F. J., 1968, Stratigraphy and structure of the Table Mountain–Mission Peak area in the Wenatchee Mountains, central Washington: University of Washington Master of Science thesis, 44 p., 1 plate.
- Sadowski, A. J.; McCosby, J. B.; Anderson, M. L.; Lau, T. R.; Steiner, Ashley; DuFrane, S. A.; Rittenour, Tammy; Housen, Bernard, 2020, Geologic map of the Ellensburg North and southern half of the Reecer Canyon 7.5-minute quadrangles, Kittitas County, Washington: Washington Geological Survey Map Series 2020-01, 1 sheet, scale 1:24,000, 25 p. text. [https://www.dnr.wa.gov/publications/ger_ms2020-01_geol_map_ellensburg_north_reecer_canyon_24k.zip]
- Sadowski, A. J.; Gilliland, A. L.; Anderson, M. L., 2021, Geologic map of the Colockum Pass SW and southern half of the Naneum Canyon 7.5-minute quadrangles, Kittitas County, Washington: Washington Geological Survey Map Series 2021-03, 1 sheet, scale 1:24,000, 23 p. text. [https://www.dnr.wa.gov/publications/ger_ms2021-03_geol_map_colockum_pass_sw_southern_naneum_canyon_24k.zip]
- Sadowski, A. J.; Lau, T. R., 2022, Geologic map of the Colockum Pass SE 7.5-minute quadrangle, Kittitas County, Washington: Washington Geological Survey Map Series 2022-05, 1 sheet, scale 1:24,000, 21 p. text. [https://www.dnr.wa.gov/publications/ger_ms2022-05_geol_map_colockum_pass_se_24k.zip]
- Sawlan, M. G., 2018, Alteration, mass analysis, and magmatic composition of the Sentinel Bluffs Member, Columbia River flood basalt province: *Geosphere*, v. 14, no. 1, 18 p. [https://doi.org/10.1130/GES01188.1]
- Schmincke, Hans-Ulrich, 1964, Petrology, paleocurrents, and stratigraphy of the Ellensburg Formation and interbedded Yakima Basalt flows, south-central Washington: Johns Hopkins University Doctor of Philosophy thesis, 426 p.
- Schmincke, Hans-Ulrich, 1967a, Stratigraphy and petrography of four upper Yakima Basalt flows in south-central Washington: *Geological Society of America Bulletin*, v. 78, no. 11, p. 1385–1422. [https://doi.org/10.1130/0016-7606(1967)78[1385:SAPOFU]2.0.CO;2]
- Schmincke, Hans-Ulrich, 1967b, Graded lahars in the type sections of the Ellensburg Formation, south-central Washington: *Journal of Sedimentary Research*, v. 37, no. 2, p. 438–448. [https://doi.org/10.1306/74D716EA-2B21-11D7-8648000102C1865D]
- Schuster, J. E., compiler, 1994, Geologic map of the east half of the Yakima 1:100,000 quadrangle, Washington: Washington Division of Geology and Earth Resources Open File Report 94-12, 19 p., 1 plate. [https://www.dnr.wa.gov/Publications/ger_ofr94-12_geol_map_yakima_e_100k.zip]
- Sláma, Jiří; Košler, Jan; Condon, D. J.; Crowley, J. L.; Gerdes, Alex; Hanchar, J. M.; Horstwood, M. S. A.; Morris, G. A.; Nasdala, Lutz; Norberg, Nicholas; Schaltegger, Urs; Schoene, Blair; Tubrett, M. N.; Whitehouse, M. J., 2008, Plešovice zircon—A new natural reference material for U-Pb and Hf isotopic microanalysis: *Chemical Geology*, v. 249, no. 1–2, p. 1–35. [https://doi.org/10.1016/j.chemgeo.2007.11.005]

- Smith, G. O., 1903a, Geologic atlas of the United States—Ellensburg folio, Washington: U.S. Geological Survey Geologic Folio 86, 7 p., with maps, scale 1:125,000. [https://doi.org/10.3133/gf86]
- Smith, G. O., 1903b, Anticlinal mountain ridges in central Washington: *Journal of Geology*, v. 11, no. 2, p. 166–177. [https://www.journals.uchicago.edu/doi/pdf/10.1086/621067]
- Smith, G. A., 1988a, Neogene synvolcanic and syntectonic sedimentation in central Washington: *Geological Society of America Bulletin*, v. 100, no. 9, p. 1479–1492. [https://doi.org/10.1130/0016-7606(1988)100<1479:NSASSI>2.3.CO;2]
- Smith, G. A., 1988b, Sedimentology of proximal to distal volcanics dispersed across an active foldbelt: Ellensburg Formation (late Miocene), central Washington: *Sedimentology*, v. 35, no. 6, p. 953–977. [https://doi.org/10.1111/j.1365-3091.1988.tb01740.x]
- Polenz, Michael; Vermeer, J. L.; Legorreta Paulín, Gabriel; Tepper, J. H.; Mahan, S. A.; Cakir, Recep, 2017, Geologic map of the Littlerock 7.5-minute quadrangle, Thurston County, Washington: Washington Geological Survey Map Series 2017-01, 1 sheet, scale 1:24,000, 36 p. text. [http://www.dnr.wa.gov/publications/ger_ms2017-01_geol_map_littlerock_24k.zip]
- Staisch, Lydia; Blakely, Richard; Kelsey, Harvey; Styron, Richard; Sherrod, Brian, 2018a, Crustal structure and Quaternary acceleration of deformation rates in central Washington revealed by stream profile inversion, potential field geophysics, and structural geology of the Yakima folds: *Tectonics*, v. 37, no. 6, p. 1750–1770. [https://doi.org/10.1029/2017TC004916]
- Staisch, Lydia; Kelsey, Harvey; Sherrod, Brian; Moller, Andreas; Paces, James; Blakely, Richard; Styron, Richard, 2018b, Miocene–Pleistocene deformation of the Saddle Mountains: Implications for seismic hazard in central Washington, USA: *Geological Society of America Bulletin*, v. 130, no. 3–4, p. 411–437. [https://doi.org/10.1130/B31783.1]
- Swanson, D. A.; Wright, T. L., 1976, Guide to field trip between Pasco and Pullman, Washington, emphasizing stratigraphy, vent areas, and intracanyon flows of Yakima Basalt; Geological Society of America Cordilleran Section, 72nd Annual Meeting, Field guide no. 1: Washington State University Department of Geology, 33 p.
- Swanson, D. A.; Wright, T. L., 1978, Bedrock geology of the northern Columbia Plateau and adjacent areas. In Baker, V. R.; Nummedal, Dag, editors, *The channeled scablands—A guide to the geomorphology of the Columbia Basin*, Washington: U.S. National Aeronautics and Space Administration, p. 37–57.
- Swick, C. H., 1942, Pendulum gravity measurements and isostatic reductions: U.S. Department of Commerce Coast and Geodetic Survey Special Publication 232, 82 p.
- Sweeney, M. R.; McDonald, E. V.; Gaylord, D. R., 2017, Generation of the Palouse loess: Exploring the linkages between glaciation, outburst megafloods, and eolian deposition in Washington State. In Haugerud, R. A.; Kelsey, H. M., editors, *From the Puget Lowland to East of the Cascade Range: Geologic Excursions in the Pacific Northwest*: Geological Society of America Field Guide 49, p. 207–228. [https://www.doi.org/10.1130/2017.0049(09)]
- Tabor, R. W.; Waitt, R. B., Jr.; Frizzell, V. A., Jr.; Swanson, D. A.; Byerly, G. R.; Bentley, R. D., 1982, Geologic map of the Wenatchee 1:100,000 quadrangle, central Washington: U.S. Geological Survey Miscellaneous Investigations Series Map I-1311, 1 sheet, scale 1:100,000, with 26 p. text. [https://doi.org/10.3133/i1311]
- Telford, W. M.; Geldart, L. O.; Sheriff, R. E., 1990, *Applied Geophysics*: New York, Cambridge University Press, 770 p.
- Tolan, T. L.; Reidel, S. P.; Beeson, M. H.; Anderson, J. L.; Fecht, K. R.; Swanson, D. A., 1989, Revisions to the estimates of the areal extent and volume of the Columbia River Basalt Group. In Reidel, S. P.; Hooper, P. R., editors, *Volcanism and tectonism in the Columbia River flood-basalt province*: Geological Society of America Special Paper 239, p. 1–20. [https://doi.org/10.1130/SPE239-pl]
- U.S. Army Corps of Engineers, 2008, Yakima Training Center 2008 project, collected 10/14/2008 to 10/23/2008, 3-foot resolution, available upon request from the Yakima Training Center.
- Waitt, R. B., Jr., 1979, Late Cenozoic deposits, landforms, stratigraphy, and tectonism in Kittitas Valley, Washington: U.S. Geological Survey Professional Paper 1127, 18 p. [https://doi.org/10.3133/pp1127]
- Wells, R. E.; Weaver, C. S.; Blakely, R. J., 1998, Fore-arc migration in Cascadia and its neotectonic significance: *Geology*, v. 26, no. 8, p. 759–762. [https://doi.org/10.1130/0091-7613(1998)026<0759:FAMI-CA>2.3.CO;2]
- Wells, R. E.; McCaffrey, Robert, 2013, Steady rotation of the Cascade arc: *Geology*, v. 41, no. 9, p. 1027–1030. [https://doi.org/10.1130/G34514.1]
- Wiedenbeck, Michael; Allé, P.; Corfu, Fernando; Griffin, W. L.; Meier, Martin; Oberli, Felix; Von Quadt, Albrecht; Roddick, J. C.; Spiegel, W., 1995, Three natural zircon standards for U-Th-Pb, Lu-Hf, trace element and REE analyses: *Geostandards Newsletters*, v. 19, p. 1–23. [https://doi.org/10.1111/j.1751-908X.1995.tb00147.x]
- Williams, I. S., 1998, U-Th-Pb geochronology by ion microprobe. In McKibben, M. A.; Shanks III, W. C.; Ridley, W. I., editors, *Applications of microanalytical techniques to understanding mineralizing processes: Reviews in Economic Geology*, v. 7, p. 1–35. [https://doi.org/10.5382/Rev.07]
- Williams, Howel; Masson, P. H., 1949, Geology of the Macdoel quadrangle and circular soil structures in northeastern California: California Division of Mines and Geology, Bulletin 151, scale 1:125,000. [https://ngmdb.usgs.gov/Prodesc/proddesc_531.htm]
- Wilson, M. S.; Dyman, T. S.; Condon, S. M., 2008, Evaluation of welltest results and the potential for basin-center gas in the Columbia basin, central Washington: U.S. Geological Survey Data Series 2184-F-O, 12 p. [https://doi.org/10.3133/ds2184FO]
- Wilt, M. J.; Morrison, H. F.; Lee, K. H.; Goldstein, N. E., 1989, Electromagnetic sounding in the Columbia Basin, Yakima Washington, *Geophysics*, v. 54, no. 8, p. 952–961. [https://doi.org/10.1190/1.1442738]

Appendix A. Gravity

OVERVIEW

Lateral changes in isostatic gravity across a region result from density changes within rocks of the mid-to-upper crust. Gravity surveys are especially useful in delineating steeply dipping contacts between two rock bodies that have a large contrast in density. The goals of this gravity survey are to: (1) delineate position and geometry of density contrasts within the subsurface, (2) determine length and geometry of known structures, and (3) identify previously unknown structures.

DATA ACQUISITION

New gravity measurements (stations) from 352 individual points collected using a Scintrex CG-6 meter (Serial # 19050174) supplement 848 stations from previous studies (Sadowski and others, 2020, 2021, 2022) and 5 stations from the PACES database (now defunct; data obtained from B. Drenth, U. S. Geological Survey, written commun., 2020). The Ellensburg B base station (Nilsen, 1976) ties our data to the U.S. gravity network. Gravity station spacing at roughly 2 km generates a basic grid over a large area with 1 km spacing in areas where known structures exist or initial gravity data collection showed a significant gradient. Along modeled cross section lines, station spacing is roughly 250 m, as access warrants. A Javad Triumph-2 differential GPS unit provides the horizontal and vertical position of each station.

DATA CORRECTIONS AND PROCESSING

The proprietary Javad Justin software allows for post-processing to make differential corrections utilizing NOAA and the National Geodetic Survey's Continuously Operating Reference Stations (CORS) within 70 km of the study area. After processing, typical positional accuracy is 0.15 m in the vertical and horizontal. Where lidar-based elevations are likely higher precision than GPS elevations, we use them in our analysis. We apply the factory gravimeter calibration constants to each gravity observation, apply correction factors obtained from the Mount Hamilton calibration loop east of San Jose, CA (Barnes and others, 1969), and correct for Earth tides to produce observed gravity values. The data reference the International Gravity Standardization Net of 1971 (Morelli, 1974), and the reference ellipsoid is the Geodetic Reference System of 1967 (International Association of Geodesy and Geophysics, 1971). The assumed linear drift between base-station ties results in a maximum gravity reading error of 0.005 mGal.

Gravity data reduction formulas for the free-air anomaly are standard (for example, Telford and others, 1990; Swick, 1942) and we applied Bouguer, Earth curvature, and terrain corrections out to 166.7 km from each station to produce a complete Bouguer anomaly. Terrain corrections are a combination of a field-based component (to a radius of 68 m using the Hayford system; Plouff, 2000) and a computer-generated component (using 30-m USGS DEM grids). The complete Bouguer anomaly is further reduced to an isostatic anomaly using an Airy-Heiskanen model (Heiskanen and Vening-Meinesz, 1958), assuming a 25-km-thick crust at sea level and a crust-mantle density contrast of 400 kg/m³. All parts of the data-reduction process assume a standard reduction density of 2,670 kg/m³. Gravity readings and computed anomalies are in the Data Supplement.

Gravity data uncertainties are predominantly due to imprecise vertical position and terrain correction uncertainty. Average gravity value error from elevation uncertainty is 0.03 mGal. The uncertainty associated with terrain corrections is generally only 5–10 percent of the actual correction. Average uncertainty in steep and hilly regions is 0.12–0.23 mGal, whereas average uncertainty in flatter areas is 0.05–0.1 mGal. Based on this, we are able to interpret density variations in the upper crust that produce gravity anomalies of 0.5–1 mGal or greater.

The minimum curvature algorithms in the GIS software package Geosoft Oasis Montaj (Seequent, Inc.) transform our point isostatic anomaly data into gridded surfaces, which we use to produce 0.5 mGal contours (Fig. M1A). The maximum horizontal gradient (referred to as 'max-spots'), calculated using the curvature analysis methodology of Phillips and others (2007), quantitatively locates strong and linear boundaries between rocks in the subsurface that have substantial density differences.

Appendix B. Rock Physical Properties

OVERVIEW

Measurements of rock density and magnetic susceptibility from geologic unit samples in our map area constrain our geophysical model parameters (Appendix C). We refer to these collectively as ‘rock properties’ in the text.

DESCRIPTION OF METHOD

We collected 48 bedrock samples throughout the study area for laboratory analysis. We weighed samples using an A & D company limited FX-3000i WP analytical balance. Three measurements per sample combine to determine density: a dry weight in air, a submerged (water-saturated) weight, and a water-saturated weight in air. While these measurements produce grain density, saturated bulk density, and dry bulk density, saturated bulk density best reflects subsurface conditions and was therefore referenced for modeling. Magnetic susceptibility measurements taken with a KT10 Kappa Meter accompany rock sample density measurements, and we use the same meter to collect direct readings from outcrops where possible. We collected magnetic susceptibility measurements from 18 additional outcrops that we did not sample. In outcrops, weathering tends to replace denser minerals with less dense weathering products and turns magnetite into less magnetic minerals like hematite. In addition, our methods do not test for magnetic remanence. Therefore, all of our measured rock densities and susceptibilities from surface outcrops (Data Supplement) can be considered minimum values.

Appendix C. Quantitative Geophysical Modeling of Geologic Cross Sections

OVERVIEW

Quantitative two-dimensional forward modeling of cross sections constrained by potential-field data provides insights into subsurface unit and fault geometry that go beyond qualitative interpretations of map-view data. This technique helps provide the best possible interpretation of fault type (for example normal, reverse, or strike-slip), fault dip, and offset across the fault on units with particularly strong physical-property contrasts with surrounding rocks. This method also can identify blind faults that have little surface expression and are difficult to capture via surface geology observations.

DESCRIPTION OF METHOD

GM-SYS (provided with the Oasis-Montaj GIS software, Seequent, Inc.) provides the platform for computing the sum effect of blocks of rock in the subsurface in a two-dimensional cross section on both the gravitational and geomagnetic fields of the Earth. This is a forward-modeling method wherein the operator hypothesizes which rock types are in the subsurface, their location, and their volume, and the GM-SYS program predicts the total fields that result from that particular model. The operator's responsibility is to refine the hypothesis until the predicted potential-fields match the data measured in the field.

We start with initial simplified models, including uniform packages of sediment, sedimentary rock, metamorphic rock, or volcanic rock to fit the overall long-wavelength features in the gravity and magnetic data. Our model space extends beyond the end of the figures shown in this publication to avoid edge effects due to truncated subsurface volumes. Incrementally adding detail to our modeled stratigraphy and progressively decreasing the size of model blocks allows us to fit long wavelength anomalies first in the deeper subsurface (produced by larger-scale features deeper in the subsurface) and then fit short wavelength anomalies, particularly in the near the surface (produced by smaller scale features, in particular near the surface).

Constraints on our geophysical modeling include surface geologic observations that define the lithologies that constrain the model's surficial and near-surface parameters. Surface geologic observations also define the geologic relationships among probable stratigraphy we expect in the deeper subsurface. Structural geometries that are physically possible based on standard geologic mapping and cross-section construction techniques provide additional constraint. Lab measurements (Appendix B) of density and magnetic properties of hand samples gathered from the surface provide approximate rock properties for the purposes of modeling. Applying all these constraints reduces the number of potential hypotheses for the subsurface geometry of rocks in the cross sections. We show best-fit geophysical models for each geologic cross section on the Map Sheet.

Even within these constraints, there is still the possibility that multiple hypotheses of subsurface structure can fit the gravity and magnetic data within the accepted error. Care in the construction of models helps define which parts of the subsurface model are well-constrained with the fewest alternative hypotheses and which parts could have multiple possible geometries. In general, potential-field data provide strong constraints (including their position and dip) on simple, steeply dipping boundaries that juxtapose rocks with strong differences in physical properties. Potential-field data provide very poor constraint on horizontal boundaries or boundaries between rocks with little contrast in physical properties. Depth of sub-horizontal stratigraphic boundaries within sedimentary rocks is particularly suspect and is never well constrained without the addition of good quality well or seismic-reflection data because the depth of a boundary can trade off with the contrast in density or magnetism between the rocks on either side of the boundary.

Appendix D. Geochemistry

OVERVIEW

We analyzed volcanic rocks in the map area according to their major and trace elements using whole-rock geochemistry as determined by X-Ray Fluorescence (XRF) only. This method allows us to determine rock elemental compositions and chemostratigraphic classifications. The results of the analyses are presented in the Data Supplement.

SAMPLE COLLECTION AND PREPARATION

We collected 329 samples within, south, and east of the map area, representing a variety of CRBG volcanic cooling textures that include: colonnade, entablature, vesicular tops, hyaloclastite, platy entablature, and autobreccia. We focused on collecting the first three types, but we collected from the others where we had no better outcrop options. Samples with secondary minerals were rarely collected.

The freshest available samples were collected from outcrops with a sledgehammer. All samples were field cleaned (knapped by hand or using local bedrock exposures as anvils). Weathering rinds were removed as much as possible in the field (>90% of samples). Additional weathering rind cleaning or sample splitting (<10% of samples) was performed at the CWU rock preparation lab using a sledgehammer and steel plate. Removing weathering rinds—if present—from vesicular tops was not always possible. Samples contain varied amounts of weathering and (or) hydration seams and (or) alteration. Weathered, hydrated, or altered samples were collected and analyzed where no fresher samples were available. In general, samples submitted to the lab ranged in size from centimeter-sized chips to fist-sized fragments.

Hydration seams (“alteration seams”, as described in Supplemental File 3 of Sawlan, 2018) were not rigorously removed before sending to WSU for further preparation: crushing, pulverization/powdering, and glass-bead fusion. Laboratory-based sub-sampling (Sawlan, 2018) was not performed due to time constraints. However, we categorize most of our samples into inter-rind to inter-seam sample quality according to table S1 of Sawlan (2018).

DATA CORRECTIONS AND PROCESSING

We used the machine learning (ML) model developed by Dr. Ashley Steiner at the WSU Peter Hooper GeoAnalytical Lab to categorize GRB members, submembers, and formations without stratigraphic context. Overall, the model does a better job distinguishing formation-level units from each other (for example, Wanapum versus Grande Ronde) than member-level or submember-level units from each other. For this reason, we relied less on the ML model for member-level and submember-level classifications compared to previous years. Instead, we plotted elemental variation diagrams (TiO_2 vs. MgO , TiO_2 vs. P_2O_5 , and amounts of Zr and Cr) and used stratigraphic understanding to determine the most reasonable member and submember classifications, especially when ML classifications had low confidence values.

RESULTS

Results for 329 samples are in the Data Supplement. Limits of Determination (LOD) are also included in the column header for each respective analyte in the Data Supplement.

Appendix E. Geochronology

OVERVIEW

We analyzed sedimentary material in the map area to determine maximum depositional age (MDA) and to conduct a preliminary assessment of the provenance of detrital zircons. For this year's study we collected samples at 12 locations. Summary data for these sites are contained in Table E1; individual zircon analytical results are in the Data Supplement.

SAMPLE COLLECTION AND PREPARATION

To understand the ages of particular rock units, we collected seven samples in 2021 and five samples in 2022 for zircon age analysis. In general, we attempted to retrieve about 2–4 kg of fresh rock for each sample, making sure to minimize any contact with soil or other surface deposits, which could introduce anomalous zircons. The packaged samples were sent to ZirChron, LLC for mineral separation using the following procedure. Samples were pressure-washed with water and then disaggregated using an Electro Pulse Disaggregator (EPD, Marx generator) at 1 Hz with discharges of ~250 kV for 15 minutes. Any clasts >500 μm were crushed in a crusher or pulverizer. Using stainless steel sieves, the fraction between 350 μm and 25 μm was retained and then processed using the Wilfley water table, Frantz paramagnetic separator, and a two-step (3.00 g/cm³ and 3.32 g/cm³) heavy liquid methylene iodide separation. Approximately 100 individual zircon grains from each sample were hand selected and mounted in epoxy, polished to expose the grain centers, and regions suitable for analysis were identified from optical imaging.

ANALYTICAL METHODS

Zircon U-Pb ages from the map area were measured at the Radiogenic Isotope and Geochronology Lab (RIGL) at Washington State University using an Analyte G2 193 excimer laser ablation system coupled with a Thermo-Finnigan Element 2 single-collector inductively coupled plasma mass spectrometer. The laser parameters were 25 μm in diameter spot size, 10 Hz repetition rate, and ~5.0 J/cm² fluence. For the U-Pb measurement, we mostly followed the method of Chang and others (2006), except for the use of the 193 nm laser system instead of the 213 nm laser. A 10-second blank measurement of the He and Ar carrier gases (laser off) before each analysis was followed by 250 scans across masses ²⁰²Hg, ²⁰⁴Pb+Hg, ²⁰⁶Pb, ²⁰⁷Pb, ²⁰⁸Pb, ²³²Th, ²³⁵U, and ²³⁸U during ~30-sec-long laser ablation periods (in other words, one continuous, 30-second ablation at 10 Hz—10 shots fired per second—for ~300 laser shots). Analyses of zircon unknowns, standards, and quality control zircon grains were interspersed with analyses of external calibration standards, typically with 10–12 unknowns bracketed by multiple analyses of two different zircon standards (Plešovice and FC-1). The Plešovice standard (337 Ma; Sláma and others, 2008) was used to calibrate the ²⁰⁶Pb/²³⁸U and ²⁰⁷Pb/²³⁵U ages, and the FC-1 standard (1,099 Ma; Paces and Miller, 1993) was used for calibration of ²⁰⁷Pb/²⁰⁶Pb ages owing to its high count rate for ²⁰⁷Pb (~2–4 times higher than that of Plešovice). Zircon 91500 (1,065 Ma; Wiedenbeck and others, 1995; n=28 ²⁰⁷Pb/²⁰⁶Pb age=1,063 ±2.4/-5.0 Ma), Fish Canyon Tuff (~27.5 Ma; Lanphere and Baadsgaard, 2001; n=35 ²⁰⁶Pb/²³⁸U age=27.9 ±0.1/-0.2 Ma) and Temora2 (417 Ma; Black and others, 2004, n=48 ²⁰⁶Pb/²³⁸U age=417.0 ±1/-1 Ma) were used as quality control standards. Data were processed offline using the Iolite software (Paton and others, 2011). Common Pb correction was performed using the ²⁰⁷Pb method (Williams, 1998). Plots were calculated using Isoplot 4.16 (Ludwig, 2012). Zircon U-Pb data are reported in the Data Supplement.

RESULTS

We report results for samples collected in the summer of 2021 (see Appendix C of Sadowski and others, 2022) and 2022. Samples collected in 2021 are included here so we can publish them in the quadrangle they were collected in. Summary data for 12 geochronology sites are contained in Table E1; individual zircon analytical results are in the Data Supplement.

Table E1. U-Pb ages from the Kittitas and East Kittitas 7.5-minute quadrangles. MDA is 'maximum depositional age.' Full analytical data are available in the Data Supplement.

Site ID	GD01	Analysis of 114 zircon grains from a fossiliferous (leaves) micaceous siltstone to fine sandstone in the northeast portion of the East Kittitas quadrangle. Sample lacks Miocene zircons and the youngest single zircon yielded an age of 48.93 ± 1.89 Ma and is interpreted as the maximum depositional age. Age spectrum contains abundant pre-Cenozoic zircons. The sample is from an outcrop that directly underlies a curvilinear contact with Wanapum Basalt on the north side of Vantage highway. We infer a Miocene age for this sample because of this contact relationship. Sample lithology is similar to Coleman member unit Mce _C from previous work by Sadowski and others (2020, 2021), which also has abundant pre-Cenozoic zircons.
Field sample ID	Cpa109	
Map unit	Mcev	
TRS location	Sec. 7, T17N R21E	
Latitude (degrees)	46.9790300°N	
Longitude (degrees)	120.2591824°W	
Elevation (ft)	2,390	
Age $\pm 2\sigma$		No older than 48.93 ± 1.89 Ma (MDA, youngest single grain)

Site ID	GD02	Analysis of 109 zircon grains from a crossbedded variably micaceous sandstone in the eastern portion of the East Kittitas quadrangle. The youngest single zircon yielded an age of 16.25 ± 0.40 Ma, is the only Miocene zircon, and is interpreted to represent the oldest possible age of the deposit. Age spectra contains abundant pre-Cenozoic zircons. The outcrop from near the top of a 40 ft cliff directly under Wanapum Basalt and over Grande Ronde Basalt located west of the Palouse to Cascades State Park Trail. Sample lithology is similar to Coleman member unit Mce _C from previous work by Sadowski and others (2020, 2021), which also has abundant pre-Cenozoic zircons.
Field sample ID	Eka183v2	
Map unit	Mcev	
TRS location	Sec. 25, T17N R20E	
Latitude (degrees)	46.9403345°N	
Longitude (degrees)	120.2690159°W	
Elevation (ft)	2,284	
Age $\pm 2\sigma$		No older than 16.25 ± 0.40 Ma (MDA, youngest single grain)

Site ID	GD03	Analysis of 110 zircon grains from an ashy siltstone to fine sandstone from the central portion of the East Kittitas quadrangle. The youngest single zircon yielded an age of 15.11 ± 0.47 Ma. We report the weighted mean of the youngest population of zircons, 15.96 ± 0.048 Ma (MSWD=3.5, n=73/110), which we interpret as the maximum depositional age. We report the youngest population rather than youngest single grain because the site's Miocene zircons have 2 sigma uncertainties on average about half as large as those from GD04 and the first peak age is more compatible with the eruptive age from site GD05. Age spectra lacks abundant pre-Cenozoic zircons. Outcrop exposure is along an unnamed canal road underlying the Wanapum Basalt. The outcrop is widespread, low-lying, and bare of vegetation.
Field sample ID	Eka085	
Map unit	Mcev	
TRS location	Sec. 21, T17N R20E	
Latitude (degrees)	46.9528279°N	
Longitude (degrees)	120.3351795°W	
Elevation (ft)	2,037	
Age $\pm 2\sigma$		No older than 15.96 ± 0.048 Ma (MDA, youngest population)

Site ID	GD04	Analysis of 100 zircon grains from a pumiceous sandstone directly underlying Wanapum Basalt in the northwest portion of the East Kittitas quadrangle. The youngest single zircon yielded an age of 14.59 ± 1.26 Ma. This grain has a large uncertainty and instead we choose to report the first peak weighted mean age of 15.896 ± 0.093 (MSWD=1.6, n=76/100), which we interpret as the maximum depositional age. We report the youngest population rather than the youngest single grain because the sample's Miocene zircons have large 2 sigma uncertainties. Age spectra lacks abundant pre-Cenozoic zircons. Sample from the south facing railroad cut along the Palouse to Cascades State Park Trail east of Prater Rd.
Field sample ID	Eka123	
Map unit	Mcev	
TRS location	Sec. 8, T17N R20E	
Latitude (degrees)	46.9741188°N	
Longitude (degrees)	120.3545771°W	
Elevation (ft)	1,855	
Age $\pm 2\sigma$		No older than 15.90 ± 0.09 Ma (MDA, youngest population)

Site ID	GD05	Analysis of 103 zircon grains from a poorly welded to unwelded weakly porphyritic lapilli tuff in the central East Kittitas quadrangle. The youngest single zircon yielded an age of 14.61 ± 0.64 Ma. Given the pyroclastic origin of the sample, we interpret an eruptive age of 15.946 ± 0.082 Ma from the youngest population (MSWD=3, n=80/103). Age spectra lacks abundant pre-Cenozoic zircons. The outcrop is on a quarry road adjacent to a basalt quarry and above outcrops of sandstone. Exposure is low on the eastern roadside and bluish gray with some bleaching where in contact with the overlying basalt. Notably, our eruptive age is compatible with a high precision ID-TIMS age of 16.066 ± 0.04 Ma from Kasbohm and Schoene (2018) for the Vantage Member.
Field sample ID	Eka128	
Map unit	Mcev	
TRS location	Sec. 8, T17N R20E	
Latitude (degrees)	46.9808919°N	
Longitude (degrees)	120.3569669°W	
Elevation (ft)	1,954	
Age $\pm 2\sigma$		15.95 ± 0.08 Ma (eruptive age, youngest population)

Table E1 continued.

Site ID	GD06	<p>Analysis of 107 zircon grains from a laminated (ashy>diatomaceous?) siltstone in the central portion of the East Kittitas quadrangle. The youngest single grain is reported and we interpret it as the maximum depositional age. Sample contained no Miocene zircons and overlies the Frenchman Springs Member.</p> <p>Age spectra has abundant pre-Cenozoic zircons.</p> <p>Exposure is near the mouth of Wippel Creek along a canal road on high where North Branch Canal meets Turbine Ditch. Outcrop is light gray to white and on the north side within the canal. Outcrop material was sampled from above the canal's water level when the canal was seasonally drained in fall 2021. Sampling was careful to avoid introduction of zircon contamination in this canal setting, and we are not sure if we were successful.</p>
Field sample ID	Eka082	
Map unit	Mcelc	
TRS location	Sec. 33, T17N R20E	
Latitude (degrees)	46.9231039°N	
Longitude (degrees)	120.3339359°W	
Elevation (ft)	2,020	
Age $\pm 2\sigma$		No older than 46.04 ± 0.6 Ma (MDA, youngest single grain)

Site ID	GD07	<p>Analysis of 111 zircon grains from a micaceous sandstone in the southeast portion of the Kittitas quadrangle. The youngest single zircon yielded an age of 14.82 ± 0.36 Ma and is interpreted to represent the maximum depositional age of the deposit. The weighted mean age of the youngest population is 15.52 ± 0.04 (MSWD=5.1, n=64/111).</p> <p>Age spectra has some pre-Cenozoic zircons with a fair number of Precambrian zircons.</p> <p>Sample is from an outcrop on the I-82/US 97 southbound rest stop near Vanderbilt Gap. Exposure is directly underlying the Roza Member and directly overlying the Frenchman Springs Member. We infer a Miocene age.</p>
Field sample ID	KEks009	
Map unit	Mcelc	
TRS location	Sec. 10, T16N R19E	
Latitude (degrees)	46.8879175°N	
Longitude (degrees)	120.4324657°W	
Elevation (ft)	2,603	
Age $\pm 2\sigma$		No older than 14.82 ± 0.36 Ma (MDA, youngest single grain)

Site ID	GD08	<p>Analysis of 106 zircon grains from a coarse to medium sandstone under a pumice- and mafic-rich (hornblende+biotite?) tephra on the northern flank of Manastash Ridge in the southern portion of the Kittitas quadrangle. The youngest single zircon yielded an age of 10.38 ± 0.35 Ma and is interpreted to represent the oldest possible age of the deposit. The youngest population is 10.95 ± 0.05 Ma (MSWD=4.2, n=34/106).</p> <p>Age spectra has some pre-Cenozoic zircons, most of which are younger than 250 Ma.</p> <p>Outcrop is on an east-facing exposure along a dirt road and overlies laminated and crossbedded siltstone and structureless mudstone.</p>
Field sample ID	KEkL240	
Map unit	Mvce	
TRS location	Sec. 4, T16N R19E	
Latitude (degrees)	46.9069844°N	
Longitude (degrees)	120.4495505°W	
Elevation (ft)	1,881	
Age $\pm 2\sigma$		No older than 10.38 ± 0.35 Ma (MDA, youngest single grain)

Site ID	GD09	<p>Analysis of 56 zircon grains from a pumice separate within a re-worked(?) tephra on the northern flank of Manastash Ridge in the southern portion of the Kittitas quadrangle. The youngest single zircon yielded an age of 8.11 ± 0.36 Ma. We report the weighted mean of the youngest population age to be 8.72 ± 0.04 Ma (MSWD=5.9, n=41/56), and interpret this as an eruptive age of the pumice fragments.</p> <p>Age spectra lack abundant pre-Miocene and pre-Cenozoic zircons probably because sample is a non-detrital pumice separate.</p> <p>Exposure is along an unnamed canal road and sample is from an outcrop that directly overlies a thin marker bed of accretionary lapilli tuff, which would also be a suitable target for U-Pb dating if not for lack of time.</p>
Field sample ID	KEks261rv3	
Map unit	Mvce	
TRS location	Sec. 33, T17N R19E	
Latitude (degrees)	46.9219794°N	
Longitude (degrees)	120.4654359°W	
Elevation (ft)	1,620	
Age $\pm 2\sigma$		8.72 ± 0.04 Ma (eruptive age (?), youngest population)

Site ID	GD10	<p>Analysis of 111 zircon grains from a parallel laminated medium-grained sandstone at Potato Hill in the western portion of the Kittitas quadrangle. The youngest single zircon yielded an age of 5.41 ± 0.14 Ma and is interpreted to represent the oldest possible age of the deposit. The youngest population is 5.68 ± 0.07 Ma (MSWD=10, n=7/111).</p> <p>Age spectra has abundant Mesozoic zircons and lacks abundant Precambrian zircons.</p> <p>Outcrop exposure is on the west side of Potato Hill and sample is from a ~1 m thick sandstone lens that overlies a conglomeratic facies that includes meter-scale rip-up clasts of basaltic sandstone. The sand lens sample directly underlies rusty orangish brown gravels. Note this sample underlies a ^{26}Al-^{10}Be isochron burial age of 2.9 ± 0.1 Ma (Bender and others, 2016) from these rusty brown gravels interpreted to be the Thorp Gravel.</p>
Field sample ID	KEks269v4	
Map unit	Mcge	
TRS location	Sec. 20, T17N R19E	
Latitude (degrees)	46.9423159°N	
Longitude (degrees)	120.4948064°W	
Elevation (ft)	1,477	
Age $\pm 2\sigma$		No older than 5.41 ± 0.14 Ma (MDA, youngest single grain)

Table E1 continued.

Site ID	GD11	<p>Analysis of 112 zircon grains from a sandstone lens in the southern portion of the East Kittitas quadrangle. The youngest single zircon yielded an age of 5.22 ± 0.78 Ma and is interpreted to represent the oldest possible age of the deposit. The youngest population is 6.15 ± 0.02 Ma (MSWD=2.6, n=94/112). We report the youngest single grain to represent the MDA because it is slightly younger than the youngest population.</p> <p>Age spectra lack abundant pre-Cenozoic zircons.</p> <p>Exposure is southwest facing and sample comes from the ~1 m thick light brown sand lens directly under the hillcapping basaltic gravels. Additional gravels are common below the sampled horizon too.</p>
Field sample ID	KEks220	
Map unit	Mcge	
TRS location	Sec. 16, T16N R20E	
Latitude (degrees)	46.8803356°N	
Longitude (degrees)	120.3248831°W	
Elevation (ft)	1,907	
Age $\pm 2\sigma$		No older than 5.22 ± 0.78 Ma (MDA, youngest single grain)

Site ID	GD12	<p>Analysis of 104 zircon grains from a fine-grained lahar (or volcanoclastic siltstone?) in the northeastern portion of the Kittitas quadrangle. The youngest single zircon yielded an age of 3.26 ± 0.18 Ma and is interpreted to represent the oldest possible age of the deposit. The youngest population is 3.62 ± 0.01 Ma (MSWD=2.9, n=69/104). We report the youngest single grain to represent the MDA because it is slightly younger than the youngest population.</p> <p>Age spectra lacks abundant pre-Cenozoic zircons.</p> <p>The outcrop is a steep, west-facing cliff along Caribou Road. Sample is from midway up the ~5 m cliff.</p>
Field sample ID	Eka136	
Map unit	Rcg	
TRS location	Sec. 1, T17N R19E	
Latitude (degrees)	46.9909962°N	
Longitude (degrees)	120.3969626°W	
Elevation (ft)	1,718	
Age $\pm 2\sigma$		No older than 3.26 ± 0.18 Ma (MDA, youngest single grain)